

# Edge-wave phase-shifts versus normal-mode phase-tilts in an Eady problem with a sloping boundary

J. Mak\*

*Department of Ocean Science, Hong Kong University of Science and Technology, Hong Kong  
Center for Ocean Research in Hong Kong and Macau,  
Hong Kong University of Science and Technology, Hong Kong and  
National Oceanography Centre, Southampton, UK*

N. Harnik and E. Heifetz

*Porter school of the Environment and Earth Sciences, Tel Aviv University, 69978, Israel*

G. Kumar†

*Department of Ocean Science, Hong Kong University of Science and Technology, Hong Kong  
Center for Ocean Research in Hong Kong and Macau,  
Hong Kong University of Science and Technology, Hong Kong and  
Department of Mathematics, Faculty of Science and Technology (Icfaitech),  
ICFAI Foundation for Higher Education, Hyderabad 501203, Telangana, India*

E. Q. Y. Ong

*Climate Change Research Centre, Australian Centre for Excellence in Antarctic Science,  
University of New South Wales, Sydney, NSW, Australia and  
Australian Research Council Centre of Excellence for Climate Extremes,  
University of New South Wales, Sydney, NSW, Australia*

One mechanistic interpretation of baroclinic instability is that of mutual constructive interference of Rossby edge-waves. While the two edge-waves and their relative phase-shifts are invoked as part of the mechanistic interpretation, for example in relation to suppression of baroclinic instability over slopes, the phase-tilts of the related normal modes are often presented instead. Here we highlight the differences between edge-wave phase-shifts and normal-mode phase-tilts, in the context of an Eady problem modified by the presence of a sloping boundary. The resulting problem remains tractable analytically, and the interacting Rossby edge-waves can be asymmetric, in contrast to the standard Eady case. We argue and present evidence that the normal-mode phase-tilt is potentially a misleading quantity to use, and edge-wave phase-shifts should be the ones that are mechanistically relevant. We also provide a clarification for the mechanistic rationalization for baroclinic instability in the presence of slopes (such as suppression of growth rates) that is valid over all parameter space, in contrast to previous attempts. We further present evidence that there is a strong correlation between quantities diagnosed from the GEOMETRIC framework with the edge-wave phase-shifts, but not the normal-mode phase-tilts. The result is noteworthy in that the geometric framework makes no explicit reference to the edge-wave structures in its construction, but the correlation suggests that in problems where edge-wave structures are not so well-defined or readily available, the GEOMETRIC framework should still capture mechanistic and dynamical information. Some implications for parameterization of baroclinic instability and relevant eddy-mean feedbacks are discussed. For completeness, we also provide an explicit demonstration that the linear instability problem of the present modified Eady problem is parity-time symmetric, and speculate on some suggestive links between parity-time symmetry, shear instability, and the edge-wave interaction mechanism.

## I. INTRODUCTION

Baroclinic dynamics and its turbulence are ubiquitous features in rotating stratified systems, playing a key role in systems such as the Earth's ocean and atmosphere as well as other geophysical/astrophysical systems, for the associated transport of buoyancy and impacts the overturning circulation [e.g., 1–10]. Understanding the mechanisms and conditions for instability, its transition to turbulence and its eventual saturation is of interest in understanding and modeling of the evolution in the relevant rotating stratified systems.

It is not too controversial to say the subject of baroclinic instability is rather well-understood at least in the hydrodynamic regime, where the linear instability phase of idealized models have analytical solutions [e.g., 11–14], and general stability

---

\* julian.c.l.mak@googlemail.com

† gautam.kmr10@zohomail.in

theorems may be derived [e.g., 15–18]. The nonlinear phase can also be tackled, mostly by numerical means [e.g., 19–28]. Often of interest in those cases are the associated statistics such as meridional eddy buoyancy fluxes (baroclinic instability usually leads to poleward eddy buoyancy flux in order for reduction of available potential energy [e.g., 1]), which plays a role in the eddy-mean interaction in the relevant rotating stratified systems, and informs on the parameterization in numerical general circulation models. A link that has been of particular interest is that of *quasi-linear control*, i.e., to what degree does the linear instability characteristics have an imprint on the nonlinear dynamics. While one could argue that the processes that are being parameterized are inherent manifestations of the nonlinear dynamics, and there is no strong reason that the relevant linear analysis should play any role, the fact remains that there does appear a relation between the two [e.g., 29–33]. A piece of work of relevance here is the GEOMETRIC framework of [34, 35] (see also [36, 37]), which has highlighted a link between the associated eddy fluxes in terms of geometric quantities associated with eddy variance ellipses (such as anisotropy factors and angles) and the linear instability properties. The scalings provided from the GEOMETRIC framework has found particular skill in the parameterization of eddy buoyancy fluxes in numerical ocean general circulation models [e.g., 38–40].

In the present case we are interested in the instability characteristics of baroclinic instability in the presence of a slope, where ‘slope’ is broadly interpreted to mean a slope as a physical boundary (e.g. topography in the atmosphere and/or ocean), or motion in the presence of an impermeable surface arising from the relevant fluid properties (e.g., adiabatic flow above/below a sloping isentrope in planetary atmospheres, magnetic field effects in the solar tachocline above the radiative zone). Analogous investigations of classical baroclinic instability in the presence of weak slopes in the linear and nonlinear regime exist, and is of particular relevance in the field of oceanography. The presence of continental slopes is generally seen to suppress eddy buoyancy fluxes over the slope regions [e.g., 41–58], with consequences for the material exchange between the shelf and open ocean environment. One possible contributing factor for the observed suppression over slope regions is that the linear instability is itself suppressed and/or less efficient over regions with slopes [e.g., 41–45, 47, 53, 54]. In relation to the GEOMETRIC parameterization, the work of [56] has found, by diagnoses, that a tuning parameter  $\alpha$  normally interpreted as a baroclinic eddy efficiency for the feedback onto the mean state [e.g., 38] is suppressed over the slope regions. A slope suppressed  $\alpha$  has been found to lead to improvements in idealized prognostic calculations [57], providing additional evidence that there should be reduced eddy feedback over slopes. The links between the observed suppression of this  $\alpha$  parameter and possible links with linear stability analysis are to be clarified, and is one of the goals of the present work.

Why exactly are baroclinic instabilities suppressed over slopes? For this, we note first that, in the absence of slopes, a kinematic/mechanistic interpretation of baroclinic instability is normally given in terms of a pair of counter-propagating Rossby edge-waves [e.g., 59–61] (although the concept of instability arising from a constructive interference of edge-waves appears to hold for general shear instabilities [e.g., 62–66]). If the edge-waves are the building blocks of the instability, then knowing how the edge-waves interact and form the instability should help with parameterization efforts. The mechanism is illustrated in Fig. 1a for the classical Eady problem [12], and proceeds as follows:

1. Rossby waves are supported on potential vorticity (PV) gradients, and in the standard Eady set up, PV is only non-zero and localized at the upper and lower boundaries, associated with buoyancy anomalies [e.g. 1], hence Rossby edge-waves;
2. the Rossby edge-waves carry PV anomalies, and the self-induced PV anomalies have associated with it a velocity (via PV inversion, cf. [60]), such that the edge-waves are *counter*-propagating against the background mean flow;
3. the waves interact with each other, and depending on the phase-shift of the edge-waves, can lead to mutual amplification of the wave displacement (the theoretical optimum being quarter of a wavelength or  $\pi/2$  out of phase), as well as some hindering/helping of the other wave’s propagation;
4. the counter-propagation against the mean flow and the mutual interaction between the waves can lead to a phase-locked configuration, and if the phase shift is also conducive for displacement amplification, then we have (modal) instability.

How is the counter-propagating Rossby wave mechanism modified by the presence of slopes? In Fig. 1b we show a case where the slope and the isopycnal configuration are in opposite orientations (the  $\delta < 0$  regime later), adapted from the work of [53]. In this set up, the vortex tube when moved in the meridional direction  $y$  is allowed to stretch more in the vertical direction  $z$ , and so the vortex tube strengthens more than it would relative to the flat case. Then it is perhaps clear what is going to happen in this setting: the bottom edge-wave is modified because the slope (if small) reinforces the value of the PV value at the bottom boundary, increasing the bottom PV gradient, and thus changing the characteristic of the bottom edge-wave. The work of [43] alludes to this but stops short of elaborating on the details. The work of [53] goes slightly further by arguing that, in the setting as in Fig. 1b, the bottom Rossby edge-wave would propagate *faster* (because the associated PV gradient is enhanced), the associated doppler shifted velocity  $\bar{U}_{\text{bot}} - c > 0$  must be smaller in value (here  $\bar{U}$  denotes the basic state velocity, and suffix ‘bot’ and ‘top’ have the expected meanings). In order to maintain phase-locking, we need  $\bar{U}_{\text{top}} - c$  to match the  $\bar{U}_{\text{bot}} - c > 0$ , and that can only happen if  $c$  *decreases* in value, which for Rossby waves means selecting a higher wavenumber, i.e. shorter waves, providing an explanation for the observed instability bandwidth (see Fig 2a in the  $\delta < 0$  regime).

We argue here the explanation provided by [53] is incomplete. A first issue is that the argument solely based on phase-speed matching does not extend to the converse case ( $\delta > 0$ ): the instability does not monotonically go to the longest wavelength as



the degree of asymmetry between upper and lower edge-waves (the standard Eady problem being the case with symmetric interaction). We provide an internally consistent physical rationalization of the instability mechanism, with explicit references to the phase-shift and asymmetry in the wave amplitude ratios that is valid over all parameter space. We further clarify the issue of ‘phase-shifts’, by comparing results from the edge-wave basis and a standard analysis of the streamfunction eigenfunction. In Sec. IV we demonstrate links between the quantities of interest from the GEOMETRIC framework and the edge-wave analysis, highlighting a link between the eddy angles with edge-wave phase-shifts [cf., 72], as well as providing an analysis for what contributes to the suppression to the eddy efficiency parameter  $\alpha$  that is prescribed in parameterizations. We summarize our results in Sec. V, and discuss some implications of our results for parameterization of baroclinic processes.

## II. OVERVIEW OF THE MODIFIED EADY PROBLEM

The physical set up is as illustrated in Fig. 1, for the Northern Hemisphere with Coriolis parameter  $f_0 > 0$ . We start with the quasi-geostrophic (QG) equations [e.g. 1] formulated on a  $f$ -plane with potential vorticity (PV) advection in the interior, and QG buoyancy advection on the vertical surfaces, i.e.,

$$\frac{Dq}{Dt} = 0, \quad z \in (H, -H_b), \quad \frac{Db}{Dt} = 0, \quad z = H, -H_b, \quad (1)$$

where the domain of interest is between  $z = H$  and  $z = -H_b(y)$ ,  $H_b(y)$  represents the bottom slope,  $D/Dt = \partial/\partial t + \mathbf{u} \cdot \nabla$  is the material derivative,  $\mathbf{u}$  is the geostrophic velocity with associated streamfunction  $\psi$ ,  $\nabla$  the horizontal gradient operator, and  $(x, y, z)$  denotes the zonal (East-West), meridional (North-South) and vertical co-ordinate. The PV  $q$  and QG buoyancy  $b$  are defined as

$$q = \nabla^2 \psi + \frac{\partial}{\partial z} \frac{f_0}{N_0^2} b, \quad b = f_0 \frac{\partial \psi}{\partial z},$$

where  $N_0^2 = \partial \bar{B} / \partial z$  is the buoyancy frequency associated with the prescribed background stratification, where  $\bar{B}$  is the basic state buoyancy profile to be prescribed with the basic state velocity  $\bar{U}$ . Contributions from the small slope will arise through the buoyancy equation in the advective term via  $w = \mathbf{u} \cdot \nabla H_b$ , arising from the no-normal flow condition on the bottom boundary.

We make an assumption that  $\partial H_b(y) / \partial y$  is small (more precisely, that  $(N_0 / f_0) \partial H_b / \partial y$  is of order Rossby number [e.g., 43, 53]), and that  $\partial H_b(y) / \partial y$  can be approximated by a small constant contribution only in the boundary condition at  $z = -H$ . Then, linearizing against the basic state  $\mathbf{u} = \bar{U} \mathbf{e}_x = \Lambda z$  (and so  $\bar{B} = -f_0 \Lambda y$  by thermal wind shear relation), the governing linear equations are

$$\left( \frac{\partial}{\partial t} + \Lambda z \frac{\partial}{\partial x} \right) \left( \nabla^2 \psi + \frac{f_0^2}{N_0^2} \frac{\partial^2 \psi}{\partial z^2} \right) = 0, \quad z \in (-H, H), \quad (2a)$$

$$\left( \frac{\partial}{\partial t} + \Lambda H \frac{\partial}{\partial x} \right) \frac{\partial \psi}{\partial z} - \Lambda \frac{\partial \psi}{\partial x} = 0, \quad z = H, \quad (2b)$$

$$\left( \frac{\partial}{\partial t} - \Lambda H \frac{\partial}{\partial x} \right) \frac{\partial \psi}{\partial z} - \left( \Lambda - \frac{N_0^2}{f_0} \frac{\partial H_b}{\partial y} \right) \frac{\partial \psi}{\partial x} = 0, \quad z = -H. \quad (2c)$$

Non-dimensionalizing by the horizontal length-scale  $L$ , vertical length-scale  $H$ , and time-scale  $T = L/U = L/(\Lambda H)$ , we have

$$\left( \frac{\partial}{\partial t} + z \frac{\partial}{\partial x} \right) \left( \nabla^2 \psi + F^2 \frac{\partial^2 \psi}{\partial z^2} \right) = 0, \quad z \in (-1, 1), \quad (3a)$$

$$\left( \frac{\partial}{\partial t} + \frac{\partial}{\partial x} \right) \frac{\partial \psi}{\partial z} - \frac{\partial \psi}{\partial x} = 0, \quad z = 1, \quad (3b)$$

$$\left( \frac{\partial}{\partial t} - \frac{\partial}{\partial x} \right) \frac{\partial \psi}{\partial z} - (1 - \delta) \frac{\partial \psi}{\partial x} = 0, \quad z = -1, \quad (3c)$$

where  $F^2 = (f_0 L / NH)^2$  and is related to the inverse of the Burger number. A key non-dimensional parameter in the present system is (in terms of dimensional variables)

$$\delta = \frac{\partial H_b}{\partial y} \left( \frac{N_0^2}{f_0 \Lambda} \right) = \frac{\partial H_b}{\partial y} \bigg/ \frac{-\partial \bar{B} / \partial y}{\partial \bar{B} / \partial z} = \frac{\partial H_b / \partial y}{s}, \quad (4)$$

i.e. the parameter  $\delta$  relates to the orientation of intersection between the background isopycnal slopes  $s$  with the bottom slope (a  $\delta < 0$  case is illustrated in Fig. 1b); this parameter is related to the  $\alpha_T$  parameter in [47]. With that, the case  $\delta < 0$  and  $\delta > 0$

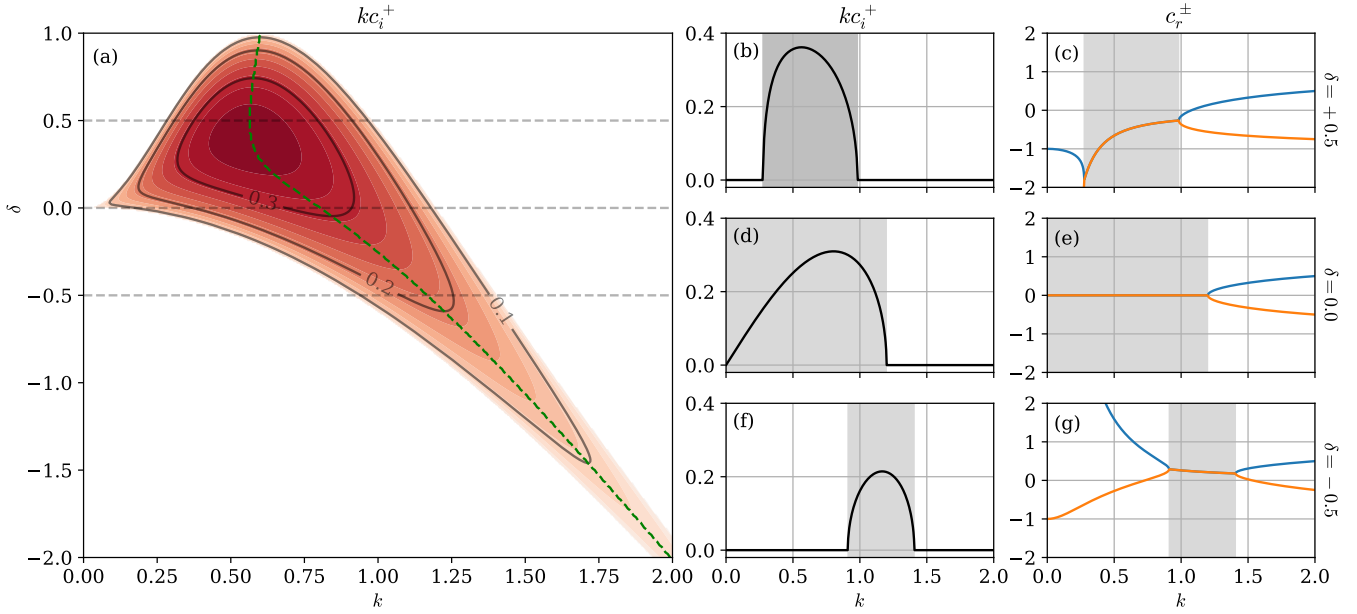


FIG. 2. General instability characteristics for the case of  $l = 0$ . (a) Growth rate as a function of the non-dimensional zonal wavenumber  $k$  and  $\delta$  parameter, with darker shadings denoting higher values, sample contours of growth rates, and the green dashed line denoting  $k_{\max}(\delta)$  where the growth rate is maximized. Also shown are the growth rates  $kc_i^+$  and phase-speed  $c_r^+$  for (b, c)  $\delta = +0.5$ , (d, e) the standard Eady problem  $\delta = 0.0$ , and (f, g)  $\delta = -0.5$ . The shaded regions in panels b-g denote the regions where there the growth rates are non-zero.

are sometimes known as retrograde or prograde configurations, although we will not be using that terminology here. One could relate the  $\delta$  parameter here to a topographic  $\beta$  term, but we refer to reader to the work of [43] for that since we do not invoke that term in this work.

With appropriate horizontal boundary choices and conditions (periodic in zonal  $x$  direction, periodic or appropriate no-normal flow boundary conditions in meridional  $y$  direction), we consider solutions of the form

$$\psi(x, y, z, t) = \tilde{\psi}(z) \exp[i(kx - \omega t)]g(y), \quad (5)$$

where  $\tilde{\psi}$  is a vertical structure function in the streamfunction,  $g(y)$  is an appropriate eigenfunction of the Laplacian operator so that  $\partial^2 g / \partial y^2 = -l^2 g$  (e.g., combinations of  $\sin ly$  and  $\cos ly$  as appropriate),  $i = \sqrt{-1}$ ,  $(k, l)$  are the zonal and meridional wavenumbers,  $\omega = kc = k(c_r + ic_i)$  is the angular frequency,  $c$  is the (complex) phase-speed; we have modal instability if  $c_i > 0$ . The modified Eady problem has zero PV signature in the interior, so the vertical structure function satisfies

$$\tilde{\psi}(z) = a \cosh \mu z + b \sinh \mu z, \quad \mu^2 = F^2(k^2 + l^2). \quad (6)$$

The constants  $a$  and  $b$  are fixed by the compatibility condition resulting from the vertical boundary conditions. Making the shorthand  $C = \cosh \mu$  and  $S = \sinh \mu$ , after some algebraic manipulation, the dispersion relation is given by

$$0 = c^2 + \frac{\delta}{2\mu} \left( \frac{C}{S} + \frac{S}{C} \right) c + \frac{\delta^2}{4\mu^2} - \left( \frac{1 - \delta/2}{\mu} - \frac{C}{S} \right) \left( \frac{1 - \delta/2}{\mu} - \frac{S}{C} \right). \quad (7)$$

Computing for  $c$  analytically or numerically, and denoting the solutions of the plus and minus branch as  $c^\pm$  for ease of discussion, plots of  $c_r^\pm$  and growth rate of the instability  $kc_i^\pm$  as a function of wavenumber  $k$  and  $\delta$  can be constructed, and a sample of this for the case  $l = 0$  is shown in Fig. 2; we will focus mostly on the  $l = 0$  case in this work since the gravest meridional mode seems to be associated with the largest growth rates at fixed  $\delta$ . Note that for our computations shown for the remainder of this work that we take  $F = 1$  for simplicity. Additionally, compared to more standard non-dimensional formulations [e.g., 1, 43, 47, 53], our values of  $k$  and  $c$  are smaller and larger by a factor of 2 respectively, but  $kc_i$  remain the same.

We make an observation that Eq. (3) is invariant under the transformation

$$\mathcal{P} : (x, y, z) \mapsto (-x, -y, -z), \quad \mathcal{T} : (t, \psi) \mapsto (-t, -\psi), \quad (8)$$

so the system is parity-time ( $\mathcal{PT}$ ) symmetric, where parity refers to a flipping or mirroring of space, while time symmetry refers to reversal of time [67–70]. Note that we regard  $\delta$  as a given and prescribed parameter of the system, so  $\delta$  does not transform

under  $\mathcal{P}$ . The fact that the equations are  $\mathcal{PT}$  symmetric implies the solution spectrum has certain properties (e.g., Fig. 2b-g), and has very suggestive links for shear instability as well as the edge-wave interpretation for shear instabilities. The details are somewhat of a digression, and we refer the reader to Appendix A for details.

There are a few features that may be observed from Fig. 2:

1. when  $\delta = 0$  and there is instability,  $c_r^\pm = 0$ ;
2. when  $\delta \neq 0$  and there is instability,  $c_r^+ = c_r^-$ , and if  $\delta > 0$ ,  $c_r^\pm < 0$  (and vice-versa for  $\delta < 0$ );
3. there is no instability for  $\delta \geq 1$ , but instability seems to persist for  $\delta < 0$ ;
4. relative to the standard  $\delta = 0$  case, the most unstable wavelength  $k_{\max}$  decreases somewhat for  $\delta > 0$ , but persistently increases for  $\delta < 0$ , with the unstable bandwidth shifting to larger wavenumbers.

A test of the wave interaction interpretation would be whether we are able to rationalize the changes in the instability characteristics via changes to the properties of these edge-waves that is valid over the whole parameter space.

The first point simply arises from our choice of problem formulation, where our domain goes from  $z = \pm 1$  and our velocity profile is anti-symmetric about  $z = 0$  (cf.  $c_r^\pm = (\bar{U}_{\text{top}} + \bar{U}_{\text{bot}})/2 = 0.5$  with the more standard formulations and choice of non-dimensionalization in other works [e.g., 1, 43, 47, 53]). The second point relates to the first point, and together with the third point can be rationalized as follows. Noting first that, with counter-propagation of Rossby edge-waves against the mean flow, the top wave intrinsically propagates to the left, while the bottom wave would propagate to the right. Noting that  $\partial H_b/\partial y \sim \delta$ , the presence of the slope is to alter the background PV gradient on which the edge-waves are propagating (cf. Fig. 1b, via PV stretching), and in the present setting,  $\delta > 0$  counteracts while  $\delta < 0$  reinforces the PV gradient provided by the background state; mathematically this is through the  $(1 - \delta)$  term in Eq. (3). For  $\delta > 0$ , the bottom wave is *weakened* and propagates *slower* for a fixed wavenumber, and one might expect the instability has more of the characteristic of the top wave propagating *left*, resulting in an unstable mode with  $c_r^\pm < c_r^\pm(\delta = 0) = 0$ . On the other hand, for  $\delta < 0$ , the bottom wave is *strengthened* and propagates *faster* for a fixed wavenumber, the bottom wave dominates and resulting in an unstable mode with  $c_r^\pm > c_r^\pm(\delta = 0) = 0$ . These observations can be verified with standard formulations, where we have instead  $c_r^\pm \leq (\bar{U}_{\max} + \bar{U}_{\min})/2 = c_r^\pm(\delta = 0) = 0$ . The third point is also consistent with the mechanistic picture: there is no instability for  $\delta \geq 1$ , because counter-propagation is then no longer possible, but for  $\delta < 0$  counter-propagation appears to always be possible, and could in principle persist at increasing wavenumbers, albeit over a decreasing bandwidth. Some of these points were already noted by the work of [47, 53].

The fourth point however is not covered by the explanation given in [47, 53] as such (although it was neither work's main focus). Those works argue that for phase-locking the edge-wave phase-speeds must match, and therefore look for conditions where the phase-speeds match. While that argument functions well for the  $\delta < 0$  regime, it (1) fails for the opposite case of  $\delta > 0$ , where the most unstable wavenumber do not uniformly go to longer waves or smaller wavenumbers (green dashed line of Fig. 2a), and (2) does not explain the changes in the strength of instability over parameter space. The reason we will argue for is simply that *mutual edge-wave interaction matters*, is part of the solution and central to the counter-propagating Rossby wave mechanism, and cannot simply be ignored, as is done when considering simply phase-speeds can match. The associated mutual interaction leads to extra helping/hindering of the wave propagation that affects phase-locking, and strength of interaction affects the growth rates.

### III. CLARIFYING THE INSTABILITY MECHANISM IN TERMS OF ROSSBY EDGE-WAVES

#### A. edge-wave formulation in phase-amplitude variables

To quantify the impact of slopes and its modification to the background PV on the wave interaction mechanism, here we consider expressing the problems explicitly in terms of Rossby or PV edge-waves and its interaction, rather than in the streamfunction eigenfunction. The streamfunction eigenfunction  $\tilde{\psi}(z)$  as it stands is in general a tilted structure in space that could be regarded as a superposition of edge-wave structures, and the problem here is in the definition of an appropriate basis of PV edge-wave functions. While there is a general approach for constructing the PV edge-waves in terms of wave activity variables such as pseudomomentum and pseudoenergy [e.g., 18, 61, 66, 73, 74], we do not need that amount of complexity here since the edge-wave locations are well defined for the present problem. For elucidation purposes we will derive the structure and governing equations explicitly.

Consider expressing the streamfunction eigenfunction  $\tilde{\psi}(z)$  in terms of a linear superposition of untilted structures focused at the top and bottom boundary (subscript  $T$  and  $B$  respectively) such that

$$\tilde{\psi} = \tilde{\psi}_T + \tilde{\psi}_B, \quad \tilde{q} = \tilde{q}_T + \tilde{q}_B, \quad (9)$$

where tilde denotes functions that are  $z$  only. Assuming modal solutions as in (5),  $\tilde{q}$  and  $\tilde{\psi}$  are related via

$$\tilde{q} = -\mu^2 \tilde{\psi} + \frac{\partial^2 \tilde{\psi}}{\partial z^2}, \quad (10)$$

subject to the boundary conditions that

$$\left. \frac{\partial \tilde{\psi}_T}{\partial z} \right|_{z=-1} = 0, \quad \left. \frac{\partial \tilde{\psi}_B}{\partial z} \right|_{z=+1} = 0. \quad (11)$$

Denoting  $\hat{\delta}$  to be the Dirac  $\delta$ -distribution, if we take (abusing mathematical rigor somewhat)

$$\tilde{q}_B = \hat{q}_B(t) \hat{\delta}(z+1), \quad \tilde{q}_T = \hat{q}_T(t) \hat{\delta}(z-1), \quad (12)$$

i.e. PV anomaly of an edge-wave is non-zero only at the associated locations, then either by manually constructing a solution [cf. 71], or by noting that we are in effect looking for the Green's function associated with the one-dimensional Helmholtz operator (in Eq. 10) subject to homogeneous Neumann conditions (in Eq. 11), for which solutions are documented (e.g., online Green's function libraries, with appropriate changes of variable), or otherwise, the relevant solutions are

$$\tilde{\psi}_B = -\hat{q}_B \frac{\cosh \mu(1-z)}{\mu \sinh 2\mu}, \quad \tilde{\psi}_T = -\hat{q}_T \frac{\cosh \mu(1+z)}{\mu \sinh 2\mu}. \quad (13)$$

Note that, with (13),

$$\tilde{b} = \frac{\partial \tilde{\psi}}{\partial z} = \begin{cases} -\hat{q}_T, & z = +1, \\ +\hat{q}_B, & z = -1, \end{cases} \quad (14)$$

demonstrating the explicit relation between buoyancy and PV anomalies, and that the top edge-wave induces no PV anomaly at the location of the other edge-wave.

Taking  $\hat{q}_T = T e^{i\epsilon_T}$  and  $\hat{q}_B = B e^{i\epsilon_B}$ , substituting (13) into the governing equations (3b, c) and considering the real and imaginary parts lead to

$$\frac{1}{T} \frac{\partial T}{\partial t} = + \frac{k}{\mu \sinh 2\mu} \frac{B}{T} \sin \Delta\epsilon, \quad (15a)$$

$$\frac{1}{B} \frac{\partial B}{\partial t} = - \frac{k(1-\delta)}{\mu \sinh 2\mu} \frac{T}{B} \sin \Delta\epsilon, \quad (15b)$$

$$-\frac{1}{k} \frac{\partial \epsilon_T}{\partial t} = + \left[ 1 - \frac{1}{\mu \sinh 2\mu} \left( \cosh 2\mu + \frac{B}{T} \cos \Delta\epsilon \right) \right], \quad (15c)$$

$$-\frac{1}{k} \frac{\partial \epsilon_B}{\partial t} = - \left[ 1 - \frac{(1-\delta)}{\mu \sinh 2\mu} \left( \cosh 2\mu - \frac{T}{B} \cos \Delta\epsilon \right) \right], \quad (15d)$$

where we define  $\Delta\epsilon = \epsilon_T - \epsilon_B$  as the phase-shift of the edge-wave in terms of PV signature;  $\Delta\epsilon > 0$  means the top wave has a PV signature that is *lagging behind* the bottom wave PV signature (cf. Fig. 1a). The set of equations are cast in a form that is more similar to Eq. (14) of [62] for the dimensional formulation of the Rayleigh shear profile problem, but is equivalent to Eq. (7) of [71], who consider the phase-shift in terms of the buoyancy variable instead. Note that since  $\tilde{\psi} \sim -\tilde{q}$ , the phase-shift applies also to the streamfunction; contrast this to  $\tilde{v} = ik\tilde{\psi}$ , which would be shifted by  $\pi/2$ , and  $\tilde{b}$  which would be shifted instead by  $\pi$ . Here,  $k/(\mu \sinh 2\mu)$  plays the role of the vertical interaction (cf.  $e^{-k}$  in [62] for the Rayleigh profile in the barotropic setting). Taking the amplitudes  $T$  and  $B$  as positive without loss of generality, we note that we need  $\Delta\epsilon \in (0, \pi)$  for growth of edge-waves, which is consistent with what we know about baroclinic instability: an unstable mode has the PV, streamfunction and meridional flow patterns leaning *against* the shear (top signal lagging bottom signal; see Fig. 4 for example), while the buoyancy pattern leans *into* the shear corresponding to a shift by  $\pi$  [e.g., 1].

While there are four independent variables, the equations depend only on the amplitude ratios and the phase difference, and could be considered a two-dimensional dynamical system. Following the notation of [62], we define the amplitude ratio as  $\tan \gamma = T/B$ . Noting then various trigonometric identities such as

$$\frac{B^2 - T^2}{B^2 + T^2} = \cos 2\gamma, \quad \frac{B^2 + T^2}{2BT} = \frac{1}{2 \sin 2\gamma},$$

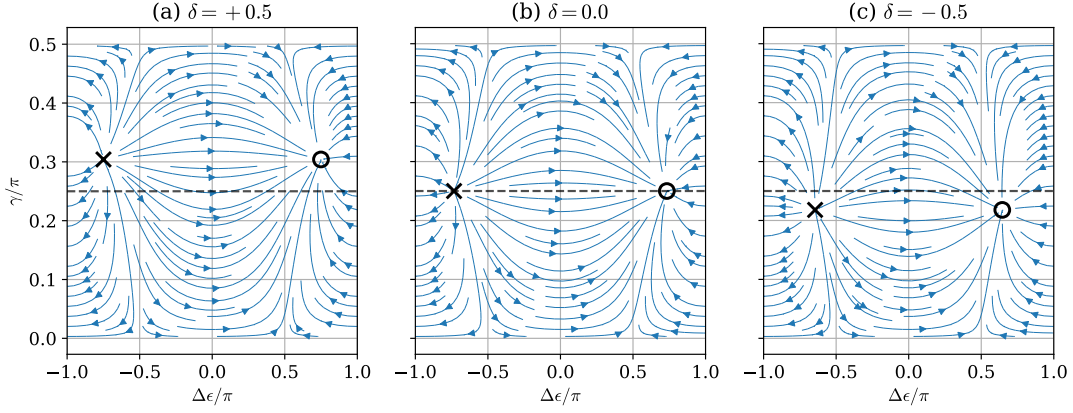


FIG. 3. Phase portrait and the fixed points of the dynamical system (stable and unstable mode marked on as a circle and cross respectively), for three choices of  $\delta$ , at wavenumber ( $k = k_{\max}(\delta)$ ,  $l = 0$ ).

(15) takes the form

$$\frac{\partial \gamma}{\partial t} = \frac{k}{\mu \sinh 2\mu} \sin \Delta\epsilon (\cos 2\gamma + \delta \sin^2 \gamma), \quad (16a)$$

$$\frac{\partial \Delta\epsilon}{\partial t} = \frac{2k}{\mu \sinh 2\mu} \left[ \left(1 - \frac{\delta}{2}\right) \cosh 2\mu - \mu \sinh 2\mu + \left(\frac{1}{\sin 2\gamma} - \frac{\delta}{2} \tan \gamma\right) \cos \Delta\epsilon \right]. \quad (16b)$$

The set of equations should be compared with Eq. (15) of [62], noting the difference in the interaction function ( $k/(\mu \sinh 2\mu)$  vs.  $e^{-k}$ ), arising from the differing physics between the systems being considered, encapsulated in the different Green's functions of the associated system.

A dynamical system could be described in terms of phase portraits [e.g., 75], and phase portraits associated with the most unstable wavenumber  $k$  (with  $l = 0$ ) for sample choices of  $\delta$  are shown in Fig. 3. Note that the stable and unstable equilibrium points of the dynamical system (repellers and attractors) are associated with the unstable and stable normal-modes respectively in the unstable bandwidth [cf. 61, 62]. As the stability boundaries are passed there is a bifurcation, and the equilibrium points become centers located at  $\gamma = 0, \pi/2$ , and  $\Delta\epsilon = \pm\pi$  (not shown), associated with neutral and freely propagating edge-waves with no change in amplitude or phase. The non-equilibrium points have been argued to correspond to non-modal growth [e.g., 62, 71], and the phase portraits indicate the regime transition in terms of edge-waves as the non-modal instabilities develop, but we leave this for the interested reader to pursue.

Focusing on the unstable modes (the attractors), we note that the associated PV phase-shifts  $\Delta\epsilon$  is *not*  $\pi/2$ , even for the  $\delta = 0$  case, which seems to contradict what is generally documented about the Eady problem having a phase-shift of  $\pi/2$  [e.g., 1]. There is in fact no discrepancy: taking the  $\delta = 0$  case as an example (i.e., standard Eady problem), we compute the values of  $\gamma$  and  $\Delta\epsilon$  associated with the stable equilibrium point and construct the edge-wave couplets as well as their sum, and these are shown in Fig. 4 (recalling  $\hat{q} = B e^{i\epsilon_B}$ , we take the reference to be  $B = 1$  and  $\epsilon_B = 0$ ). While  $\Delta\epsilon \neq \pi/2$ , their combination does lead to a phase-tilt in the *streamfunction eigenfunction*  $\Delta\epsilon_{\text{eigen}} = \pi/2$ , and the reconstructed solution can be shown to coincide exactly with the one obtained from the more standard normal-mode analysis. A non-optimal shift is realized simply because the mutual interaction from the interaction function (which is wavenumber dependent) is also part of the solution, and provides extra hindering of the wave propagation required for phase-locking [e.g., 61, 62, 65, 72]. Considerations based simply on phase-shift (or phase-tilt) and/or phase-speed matching is incomplete, because it is ignoring the interaction component.

The statement in the above paragraph holds true for different values of  $k$  and  $\delta$  (not shown). For synchronized growth of edge-waves associated with stable equilibrium points of (16), we have  $\Delta\epsilon \in (0, \pi)$  and  $\gamma \in (0, \pi/2)$ , so that the growth rate can be inferred from (15), given by

$$\sigma = \left| \frac{k}{\mu \sinh 2\mu} \frac{1}{\tan \gamma} \sin \Delta\epsilon \right| = \left| \frac{k(1-\delta)}{\mu \sinh 2\mu} \tan \gamma \sin \Delta\epsilon \right|, \quad (17)$$

which numerically coincides with that of Fig. 2a (not shown). The phase-speeds of the normal-modes  $c_r$  can also in principle be reconstructed in principle from the edge-wave basis via consideration of the self- and induced-propagation by the edge-waves [cf., 61, 66]. The edge-wave formulation here encompasses the standard formulation of the modified Eady problem, which is not surprising given it is really a reformulation of the same problem, but expressing it in a basis that allows for a mechanistic interpretation to be drawn from.



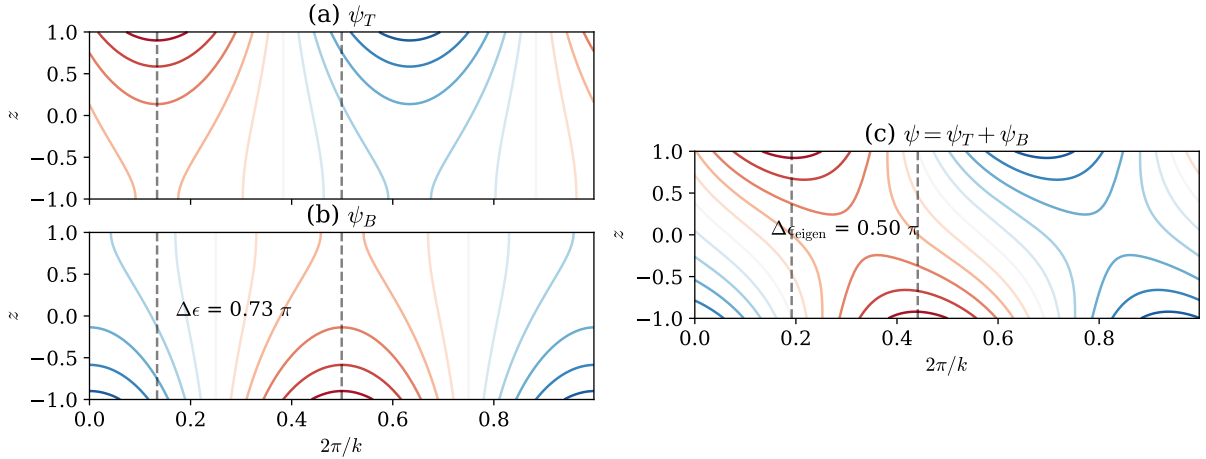


FIG. 4. Edge-waves components and the combination demonstrated for the most unstable mode of the standard Eady problem ( $\delta = 0$ ). (a, b) Associated edge-wave structure  $\psi_{T,B}$  (referenced by  $B = 1$  and  $\epsilon_B = 0$ ) given in (13) of the attracting fixed point in Fig. 3b, with  $\Delta\epsilon \neq \pi/2$ . (c) The reconstructed normal-mode  $\psi = \psi_T + \psi_B$  that has a phase-tilt  $\Delta\epsilon_{\text{eigen}} = \pi/2$ .

We show in Fig. 5 the amplitude ratios  $\gamma$  and edge-wave phase-shift  $\Delta\epsilon$  of equilibrium points of (16) associated with unstable modes. Starting first with the amplitude ratio  $\gamma$ , it is clear that  $\gamma$  only depend on  $\delta$ . The analytic expression for  $\gamma$  can be obtained by noting that, with synchronized growth and growth rate given by (17), we must have (with appropriate normalization and/or shifts in the phase)

$$\left| \frac{1}{\tan \gamma} \right| = \left| \frac{B}{T} \right| = \sqrt{1 - \delta}, \quad (18)$$

which is  $k$  independent. Notice that: (1)  $|B/T|$  is ill-defined for  $\delta > 1$ , corresponding to the case where there is no instability (since there is no counter-propagation possible for the bottom wave as the bottom background PV gradient has switched signs); (2)  $|B| = 0$  for  $\delta = 1$  for physically sound solutions (coinciding with vanishing PV gradient at the bottom); (3)  $|T| > |B|$  for  $\delta \in (0, 1)$ , i.e. weaker bottom wave; (4)  $|T| = |B|$  for  $\delta = 0$ , and there is no asymmetry in the standard Eady case; (5)  $|B| > |T|$  for  $\delta < 0$ , and there is *always* instability possible for  $\delta < 0$ . The observations are consistent with our physical expectations highlighted in the previous sections.

The behavior of  $\Delta\epsilon$  in Fig. 5c is in line with kinematic arguments from edge-waves that help or hinder each other's propagation, with implications for phase-locking. We generally need  $\Delta\epsilon \in (0, \pi)$  for constructive interference. At fixed  $\delta$ , long waves propagate faster (since these are Rossby edge-waves), and the edge-waves need to *hinder* each other to maintain phase-locking, which for instability requires  $\Delta\epsilon \in (\pi/2, \pi)$ . The converse holds for shorter waves, requiring  $\Delta\epsilon \in (0, \pi/2)$  [e.g., 61].

## B. Physical rationalization of the interacting edge-wave process

Our interpretation for the role of topographic PV on the Counter-propagation Rossby Wave mechanism is then as follows. Starting with the  $\delta < 0$  case, the bottom wave is strengthened and propagate faster, but also leads to a stronger induced velocity at the top wave. The strong interaction leads to a stronger *hindering* effect for fixed wavenumber, which will in general lead to a sub-optimal phase-shift configuration. One way to drive the configuration towards a more optimal configuration would be to go towards *shorter* waves, which offsets the increased interaction introduced by a stronger bottom wave from the fact that  $\delta < 0$  (since the interaction function goes like  $k/(\mu \sinh 2\mu)$  for the present Eady system). This also then explains the reduction in the growth rate as we shift towards shorter waves (Fig. 2a): while the efficiency could be changed via the phase-shift, the interaction strength is *decreased*. It would seem that, in the  $\delta < 0$  setting, it is *always* possible to compensate for the increase in interaction from  $\delta \rightarrow -\infty$  by reducing the interaction function via increases in  $k$ , albeit over an increasingly narrow bandwidth of wavenumbers. The phase-speeds are positive (Fig. 2g) because the bottom edge-wave propagating to the right (or eastwards) dominates over the top edge-wave.

For the  $1 > \delta > 0$  regime, the bottom wave is weakened (from (18)) and leads to a weaker hindering effect in general. What this means is that the top wave is now propagating too fast, and this effect would have to be offset by increasing the interaction function via decreasing in the wavenumber, i.e., going to longer wavelengths. However, unlike the  $\delta < 0$  case, reduction in  $k$  leads an increase in edge-wave propagation since we are dealing with Rossby edge-waves, and beyond a certain point it is

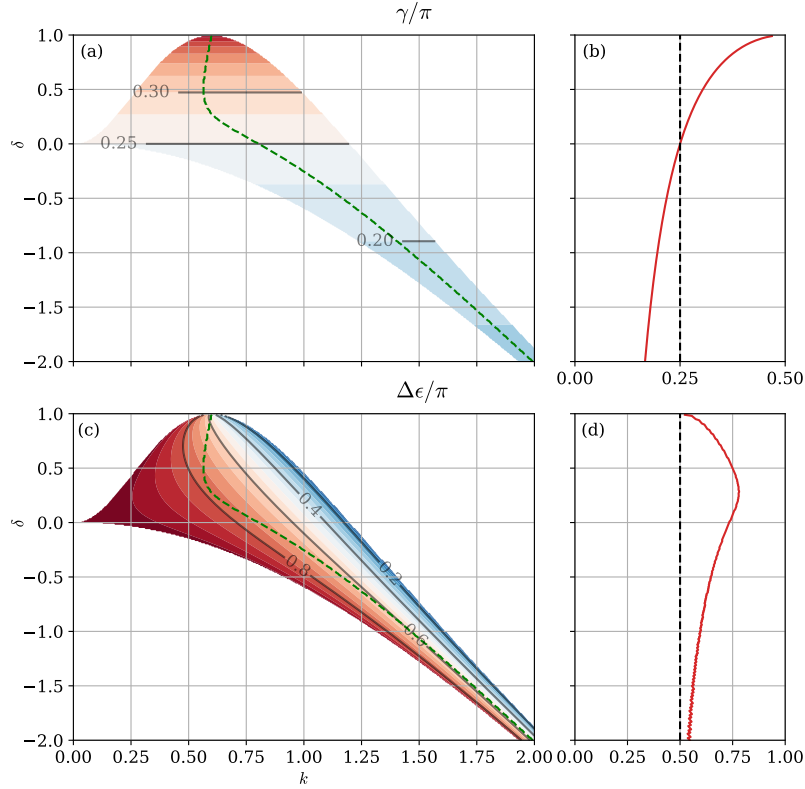


FIG. 5. (a) Normalized amplitude ratio  $\gamma$  in multiples of  $\pi$  as a function of  $k$  and  $\delta$ , and (b) the same quantity along the line of  $k_{\max}(\delta)$  (red line, with  $\gamma_{\text{eigen}}$  as faint green line); note 0.25 here denotes equal amplitude at top and bottom. (c) The normalized edge-wave phase-shift  $\Delta\epsilon$  in multiples of  $\pi$  as a function of  $k$  and  $\delta$ , and (d) the same quantity along the line of  $k_{\max}(\delta)$  (red line); note +0.5 here denotes that the top edge-wave *lags behind* the bottom edge-wave by a quarter wavelength. The line of  $k_{\max}(\delta)$  has been marked on panel (a, c) as the green dashed line.

simply not possible for the bottom wave's induced velocity and the background flow to hold the top wave into a phase-locked position, and instability is no longer possible. As  $\delta \nearrow 1$ , the PV gradient vanishes, counter-propagation is no longer possible, and no phase-locking can be achieved. Note that  $\delta \geq 1$  coincides with the non-satisfaction of the Charney–Stern condition that it is necessary for the background PV gradient to change sign in the domain in order for instability, which had previously been interpreted as a condition required for counter-propagation [e.g., 61, 74, 76]. The phase-speeds are negative (Fig. 2c) because the top edge-wave propagating to the left (or westwards) dominates over the bottom edge-wave.

### C. Analysis in terms of the instability normal-mode

Here we provide an analogous analysis to demonstrate how different the results are if the instability streamfunction eigenfunction from (5) is utilized instead. Focusing on unstable modes, given a value of  $c$ , we can obtain the coefficients  $a$  and  $b$  for the vertical structure function  $\tilde{\psi}(z)$  from (6). Given  $\tilde{\psi}(z) = \tilde{\psi}_r + i\tilde{\psi}_i$ , we can compute for a (normalized) amplitude and phase of the eigenfunction via [e.g., 1, 53]

$$|\tilde{\psi}(z)|^2 = \tilde{\psi}_r^2(z) + \tilde{\psi}_i^2(z), \quad \epsilon(z) = \arctan \frac{\tilde{\psi}_i(z)}{\tilde{\psi}_r(z)}. \quad (19)$$

Analogous to our edge-wave analysis in Sec. III, we introduce the quantities

$$\tan \gamma_{\text{eigen}} = \frac{|\tilde{\psi}(z=1)|}{|\tilde{\psi}(z=-1)|}, \quad \Delta\epsilon_{\text{eigen}} = \epsilon(z=1) - \epsilon(z=-1) \quad (20)$$

as a measure of the amplitude ratio and phase-*tilt* (rather than phase-shift) between the streamfunction eigenfunction at the top and bottom of the domain respectively. Fig. 6 shows the amplitude ratio  $\gamma_{\text{eigen}}$  and phase-tilt  $\Delta\epsilon_{\text{eigen}}$  as measured through the eigenfunction  $\tilde{\psi}(z)$ .

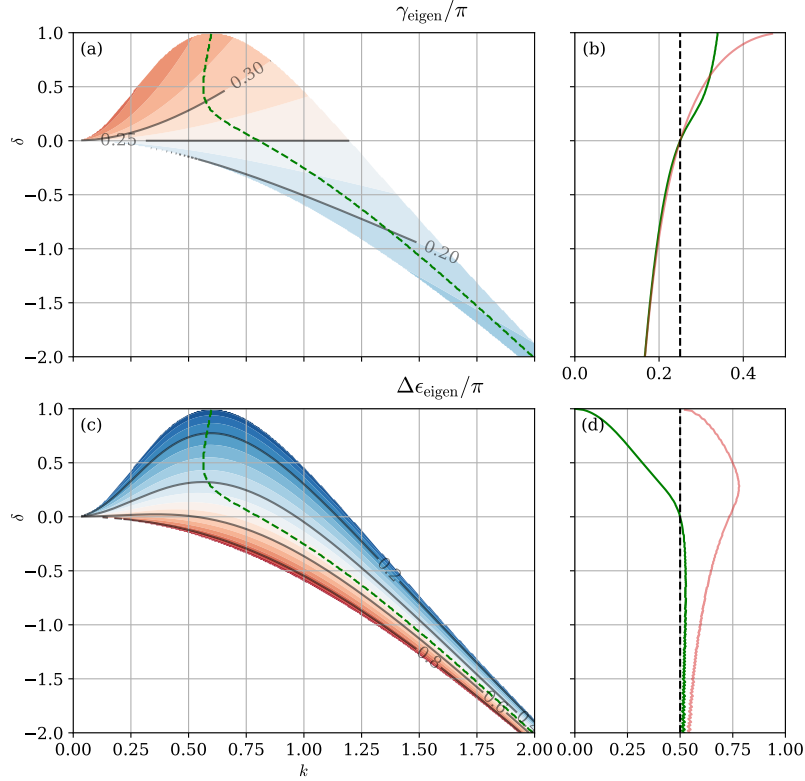


FIG. 6. Analogue of Fig. 5 but for quantities diagnosed from the normal-mode directly. (a) Normalized amplitude ratio  $\gamma_{\text{eigen}}$  in units of  $\pi$  as a function of  $k$  and  $\delta$ , and (b) the same quantity along the line of  $k_{\text{max}}(\delta)$  (green line, with  $\gamma$  from Fig. 5b as faint red line); note 0.25 here denotes equal amplitude at top and bottom. (c) The normalized phase-tilt in the streamfunction  $\Delta\epsilon_{\text{eigen}}$  in units of  $\pi$  as a function of  $k$  and  $\delta$ , and (d) the same quantity along the line of  $k_{\text{max}}(\delta)$  (green line, with  $\Delta\epsilon$  from Fig. 5d as faint red line); note +0.5 here denotes that the top edge-wave lags behind the bottom edge-wave by a quarter wavelength. The line of  $k_{\text{max}}(\delta)$  marked on as green has been marked on panel (a, c) as the green dashed line.

Starting first with the amplitude ratio, we note that the standard Eady case with  $\delta = 0$  has  $\gamma_{\text{eigen}} = \pi/4$  throughout the unstable bandwidth, i.e. the top and bottom of the normal-mode have equal amplitude, and in fact the normal-mode is symmetric about  $z = 0$  for  $\delta = 0$  (not shown; [cf., 77]). For  $\delta > 0$ ,  $\gamma_{\text{eigen}} > \pi/4$ , i.e. the normal-mode amplitude at the bottom is smaller than that at the top, and conversely for  $\delta < 0$ , consistent with results from physical expectations and edge-wave analysis. However, compared to the equivalent graph in terms of edge-waves in Fig. 6a, b, there is a wavenumber dependence in  $\gamma_{\text{eigen}}$ , when our physical argument would suggest that the amplitude ratio should only depend on  $\delta$ . The observation of  $\gamma_{\text{eigen}}$  is consistent if we remember that diagnosed quantities between two separate edge-wave structures do not necessarily need to be the same as that diagnosed from their combinations.

For the phase-tilt in the streamfunction, in the standard Eady case with  $\delta = 0$ , the maximally growing mode has  $\Delta\epsilon_{\text{eigen}} = \pi/2$ , where the top signal lags behind the bottom signal by quarter of a wavelength. As the wavenumber increases, the tilt in the normal-mode reduces, while the opposite is true as the wavenumber decreases. For  $\delta \neq 0$ , the behavior of  $\Delta\epsilon_{\text{eigen}}$  in the streamfunction is asymmetric with the sign of  $\delta$ . Notably, the most unstable wavenumber for  $\delta < 0$  has  $\Delta\epsilon_{\text{eigen}} = \pi/2$ , indicating the most unstable mode is still able to access a standard Eady-like configuration in the normal-mode, albeit with decreasing growth rate. However, while a phase-shift of  $\pi/2$  would be the optimum configuration for constructive interference in the edge-wave interaction framework [e.g., 60, 61, 71], we should note that the phase-shift  $\Delta\epsilon$  need not coincide with the phase-tilt  $\Delta\epsilon_{\text{eigen}}$  (cf. Fig. 6c, d and Fig. 5c, d). As was demonstrated in Fig. 4,  $\Delta\epsilon$  is generally not at the expected optimal because one needs to take into account of the interaction function.

One could then wonder whether there is in fact any specific meaning to the value of the phase-tilt  $\Delta\epsilon_{\text{eigen}}$ . It is certainly true that the phase-tilt  $\Delta\epsilon_{\text{eigen}}$  (as well as the PV edge-wave phase-shift) should relate to an *energetic* interpretation of the instability [e.g., §6.7.2 of 1], in relation to the fact that perturbations of meridional velocity  $v'$  and buoyancy  $b'$  should be overall positively correlated, so that the zonally averaged meridional buoyancy flux  $\overline{v'b'}$  is poleward, leading to a decrease in available potential energy. While the statement about the energetics is true, the problematic aspect is linking that to the raw value of  $\Delta\epsilon_{\text{eigen}}$ . Since in the linear instability analysis we should only be talking about rates and efficiencies, we might suspect that  $\Delta\epsilon_{\text{eigen}} = \pi/2$

would correspond to maximum efficiency in  $\overline{v'b'}$  in reducing available potential energy, i.e. maximum linear correlation. A straightforward linear regression analysis for the correlation of  $v'$  and  $b'$  over the whole spatial domain (not shown) indicates this is simply not true:  $v'$  and  $b'$  are maximally correlated in the linear sense at small  $k$ , and its dependence as a function of  $k$  and fixed  $\delta$  bears no resemblance to  $\Delta\epsilon_{\text{eigen}}$  or the growth rate plots (the scatter plots of  $v'$  against  $b'$  becomes increasingly ‘circular’ with increasing  $k$ ). The behavior of  $\overline{v'b'}$  itself (making the choice of normalizing the eigenfunction  $\tilde{\psi}(z)$  to have unit magnitude) also bears no resemblance to  $\Delta\epsilon_{\text{eigen}}$  or the growth rate: for fixed  $\delta$ , maximum  $\overline{v'b'}$  occurs at a  $k$  larger than the wavenumber at which there is maximum growth (not shown). So while  $\Delta\epsilon_{\text{eigen}}$  would in some way be related to the energetic as well as the kinematic/mechanistic view of the instability problem, it may perhaps be simpler to not attribute too much meaning to  $\Delta\epsilon_{\text{eigen}}$ . The fact that  $\Delta\epsilon_{\text{eigen}} = \pi/2$  for the most unstable mode is curious and is perhaps worthy of further exploration, but we argue here that if we are invoking the edge-wave interaction mechanism, it is perhaps quantitatively misleading or not entirely appropriate to provide evidence in terms of something that is not in edge-wave form.

#### IV. ANALYSIS IN THE GEOMETRIC FRAMEWORK

The previous section highlights subtleties when using the streamfunction eigenfunction with a mechanistic explanation, and argues that it is the edge-wave basis that are more dynamically relevant. Does that mean the instability eigenfunctions have little utility relative to the edge-wave basis? We provide a processing of the eigenfunctions in terms of the GEOMETRIC framework of [34, 35] (see also [36, 37]) that considers geometric quantities such as anisotropy factors and angles of eddy variance ellipses, and turns out to have mechanistic links with baroclinic instability (cf. the barotropic case, considered in [72]). The quantitative links between energetics and mechanistic interpretations are demonstrated here for a case where both the edge-wave basis and eddy fluxes are well-defined. The strong correlation of the geometric quantities with that diagnosed from the edge-wave framework provides a suggestion that in cases where the edge-wave basis is less well-defined (e.g., the linear Charney–Green problem, or data from the nonlinear evolution of baroclinic instability), the GEOMETRIC framework may still be utilized and has energetic and dynamical relevance.

As a recap to the work of [34–36], in the QG limit, it is known that the eddy forcing on to the mean state is determined by the object [e.g., 34]

$$\mathbf{E} = \begin{pmatrix} -M + P & N & 0 \\ N & M + P & 0 \\ -S & R & 0 \end{pmatrix}, \quad (21)$$

with

$$\begin{aligned} M &= \frac{1}{2}\overline{v'^2 - u'^2} = -\gamma_m E \cos 2\phi_m \cos^2 \lambda, & N &= \overline{u'v'} = \gamma_m E \sin 2\phi_m \cos^2 \lambda, \\ P &= \frac{1}{2N_0}\overline{b'^2} = E \sin^2 \lambda, & R &= \frac{f_0}{N_0^2}\overline{u'b'} = \gamma_b \frac{f_0}{N_0} E \cos \phi_b \sin 2\lambda, & S &= \frac{f_0}{N_0^2}\overline{v'b'} = \gamma_b \frac{f_0}{N_0} E \sin \phi_b \sin 2\lambda, \end{aligned} \quad (22)$$

where  $M, N$  denote the eddy momentum fluxes (related to the Reynolds stresses),  $R, S$  denote the eddy buoyancy fluxes (related to the form stresses),  $P$  is the eddy potential energy, and  $E = P + K$  is the total eddy energy, with the eddy kinetic energy  $K$  defined in the usual way. In the framework,  $E$  becomes the only dimensional variable, which is arbitrary up to a multiplicative constant for the linear instability problem. By contrast, the non-dimensional geometric quantities related to the eddy variance ellipses are independent of the arbitrary multiplicative constant, and are given by

$$\begin{aligned} \gamma_m &= \frac{\sqrt{M^2 + N^2}}{K}, & \gamma_b &= \frac{N_0}{2f_0} \sqrt{\frac{R^2 + S^2}{KP}}, \\ \sin 2\phi_m &= \frac{N}{\sqrt{M^2 + N^2}}, & \sin \phi_b &= \frac{S}{\sqrt{R^2 + S^2}}, \\ \frac{K}{E} &= \cos^2 \lambda, & \frac{P}{E} &= \sin^2 \lambda, & \tan^2 \lambda &= \frac{P}{K}, \end{aligned} \quad (23)$$

where the overbar denotes a mean operator (zonal average for the present work),  $\gamma_{m,b}$  are the momentum and buoyancy anisotropy parameters,  $\phi_{m,b}$  are angle parameters related to the eddy momentum and buoyancy ellipses, while  $\lambda$  is an angle relating to the eddy energy partition. Note that there is a degeneracy in the angle parameters, where for example we could define  $\phi_b$  in terms of  $\cos \phi_b = R/\sqrt{R^2 + S^2}$  as in [34].

One idea relating to parameterization of eddy fluxes is that the non-dimensional geometric parameters might be more universal and related to dynamics and/or instability characteristics, so are perhaps be easier to parameterize. For example, it is known that in barotropic/horizontal shear instabilities,  $\phi_m$  directly relates to the tilt angle of the eddy, where if the eddy tilts into the shear

we have instability, while if eddy tilts with the shear we would have the converse, with eddies fluxing momentum back into the mean state [e.g., 34, 36, 37, 72, 78]. In the present modified Eady problem, it can be demonstrated that it is the eddy buoyancy rather than momentum fluxes that are non-trivial, consistent with the present set up leading to a pure baroclinic instability. The parameters of interest are then

$$\tan 2\phi_t = \gamma_b \tan 2\lambda, \quad \gamma_t = \frac{\cos 2\lambda}{\cos 2\phi_t}, \quad (24)$$

where  $\phi_t$  and  $\gamma_t$  are the angle and anisotropy parameter of a vertical eddy in physical space [34, 36, 79]. From this, we note that we can define a non-dimensional parameter  $\alpha$  where

$$\alpha = \gamma_b \sin \phi_b \sin 2\lambda = \gamma_t \sin \phi_b \sin 2\phi_t. \quad (25)$$

The  $\alpha$  parameter is a combination of geometric parameters that closely relates to the Eady growth rate, is bounded in magnitude by unity in the QG limit [34], and is one of the tuning parameters that is at present prescribed in parameterizations of baroclinic restratification effects [e.g., 39]. An interest here is on the dependence of  $\phi_t$  and  $\alpha$  on  $\delta$ , and what is the dominant contribution to the variation of  $\alpha$ , with the possibility to aid/inform our parameterization efforts for baroclinic eddies and its feedback onto the mean state in theoretical and/or numerical models [e.g., 39, 80].

For the case of  $l = 0$ , i.e. no meridional variation,  $u' = 0$ , and so  $R = N = 0$  while  $M^2 = K$ , and so

$$\gamma_m = 1, \quad \phi_m = 0, \quad \phi_b = \pm \frac{\pi}{2}, \quad \alpha = \pm \gamma_b \sin 2\lambda = \gamma_t \sin 2\phi_t. \quad (26)$$

For the present set up it is the sign of  $\alpha$  that distinguishes whether we have instability or not, since  $\phi_b$  is defined in term of the zonal mean meridional advection of eddy buoyancy fluxes  $S$ , which is the principal interest for baroclinic instability ( $S > 0$  is poleward flux of buoyancy, and so  $\sin \phi_b$  and  $\alpha$  are both positive).

Fig. 7 shows the value of the vertically averaged  $\alpha$ , buoyancy anisotropy  $\gamma_b$  and the vertical tilt  $\phi_t$  over the unstable region in parameter space. It may be seen that  $\alpha$  correlates strongly with the growth rate (Fig. 2a), in line with the analysis of [34]. Although the values of  $\alpha$  reported here are around an order of magnitude larger than what are used in parameterizations for numerical ocean models [e.g., 39], we note that the diagnosed value here is for the linear instability analysis, whilst the values used in parameterizations are applied as averages over both energetic and quiescent regions and to mimic the feedback during the nonlinear phase. The sensitivity of  $\alpha$  to  $\delta$  is of most relevance, suggesting it should be  $\alpha$  that is decreased in value in the presence of slopes, particularly in the  $\delta < 0$  scenario (where topographic and isentropic/isopycnal slopes are opposite in orientation), consistent with a previous diagnostic result in the nonlinear regime [56].

The dominant contribution to the variation of  $\alpha$  (in both the average and pointwise sense) is principally through the buoyancy anisotropy parameter  $\gamma_b$  (see Fig 7a and c). The eddy energy partition angle parameter  $\lambda$  plays a secondary role, since  $\sin 2\lambda$  is diagnosed to be close to 1 in value in the pointwise sense (not shown). The presence of a sloping boundary would naturally be expected to force an anisotropy, and the feature of  $\alpha$  correlating well with  $\gamma_b$  and not  $\sin 2\lambda$  seems to be consistent with diagnoses from numerical simulations in a global ocean circulation model in the nonlinear regime [80], and diagnoses in the nonlinear regime of an idealized baroclinic flow over a topographic slope (personal communication with Huaiyu Wei and Yan Wang). The decreasing values of  $\gamma_b$  for fixed  $\delta$  as  $k$  is increased corresponds to a statement in the previous section that the scatter plot of  $v'$  against  $b'$  becomes increasing ‘circular’ in the same limit [cf. 34]. If we consider instead  $\alpha$  in terms of  $\phi_t$  and  $\gamma_t$ , then we see here that  $\sin 2\phi_t$  would not correlate well with  $\alpha$ , and neither would  $\gamma_t$  (not shown). So while there is a flexibility for the form of  $\alpha$  used, it would seem that, in the linear regime at least, it is  $\gamma_b$  that is more relevant, and the presence of the slopes modifies the anisotropy of the state.

The vertical eddy angle  $\phi_t$  has the behavior that  $\phi_t \searrow 0$  as  $k$  is increased for fixed  $\delta$  (Fig. 7e). One interpretation of the tilt angle could be that it is related to  $\Delta\epsilon$  of two interacting edge-waves [cf., 72, for the horizontal case], having an optimal phase shift leading to instability ( $\phi_t = \pi/4$  might be expected to be analogous to the optimum phase-shift of  $\Delta\epsilon = \pi/2$ ; cf. [72] for the case where the velocity shear is purely in the horizontal). Indeed, Fig. 7e, f showing  $\phi_t$  over parameter space resembles that of  $\Delta\epsilon$  over parameter space, as shown in Fig. 5c, d. In that sense, even though  $\phi_t$  is defined in terms of  $S \sim \overline{v'b'}$  (through the definition of  $\gamma_b$ ) and makes no reference to edge-wave structures whatsoever, there are apparent mechanistic links of  $\phi_t$  with  $\Delta\epsilon$ . In that regard,  $\phi_t$  could perhaps serve as a possible proxy for edge-wave phase-shifts that is easier to diagnose in cases where the definition of edge-wave structures becomes more ambiguous (e.g., dynamics in a nonlinear setting). Again, the phase-tilt  $\Delta\epsilon_{\text{eigen}}$  (Fig. 6c) bears little resemblance to  $\phi_t$  (Fig. 7e) nor  $\Delta\epsilon$  (Fig. 5e) over parameter space.

The diagnosed results above are presented as vertically averaged quantities, which does not demonstrate the asymmetry introduced with  $\delta$ . Examination of the full vertical profiles does in fact show the quantities to be increasingly concentrated towards the lower boundary when  $\delta < 0$  (and vice-versa), consistent with the known behavior of  $\gamma$  in (18) and Fig. 5a, the lower edge-wave being the increasingly dominant contribution (not shown). We close this section with a note that the above results should be interpreted with the caveat that the diagnoses are in the linear and nonlinear regime respectively, and the two are not necessarily directly comparable (e.g., it is not obvious that the instability has to leave a strong imprint on the nonlinear eddy fluxes locally).

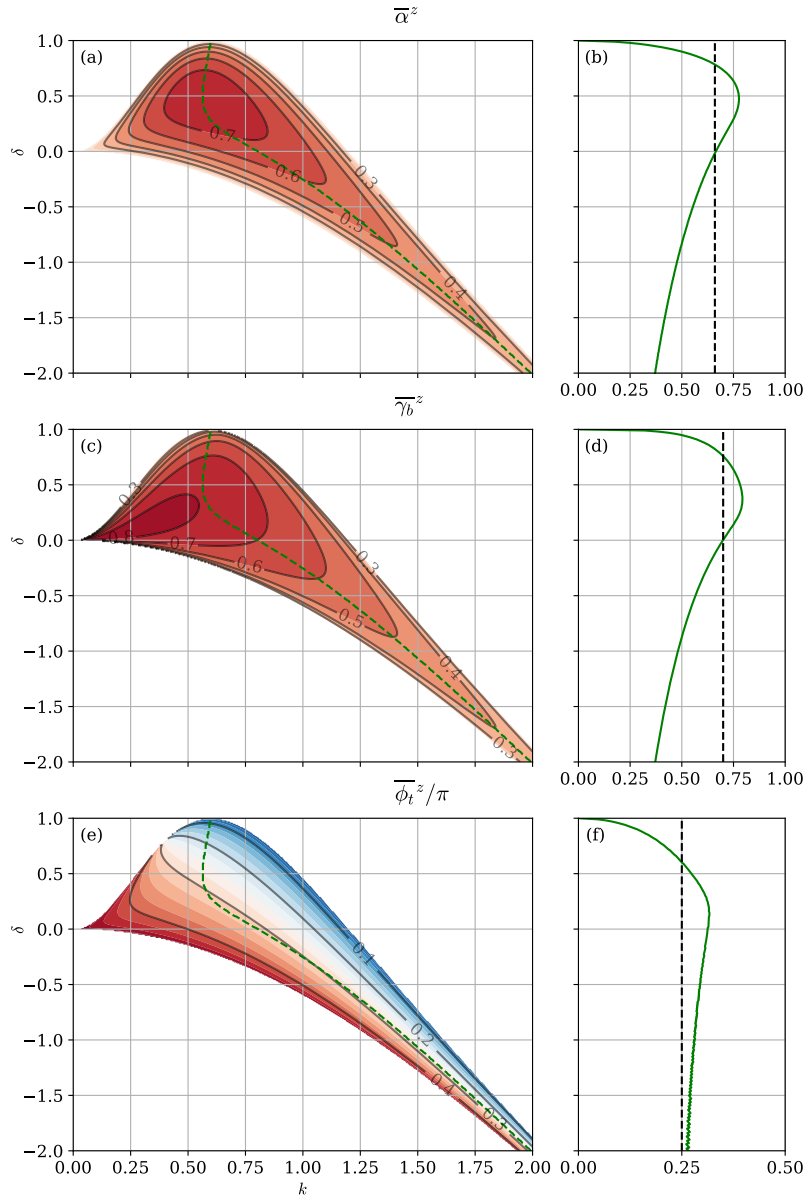


FIG. 7. Vertically averaged (a)  $\overline{\alpha}^z = \overline{\gamma}_b \sin 2\lambda^z$  (c) buoyancy anisotropy factor  $\overline{\gamma}_b^z$  and (e) vertical tile angle  $\overline{\phi}_t^z$  (in multiples of  $\pi$ ) as a function of  $k$  and  $\delta$ , and (b, d, f) the respective quantities along the line of  $k_{\max}(\delta)$ . The line of  $k_{\max}(\delta)$  marked on as green has been marked on panel (a, c, e) as the green dashed line.

## V. CLOSING REMARKS

### A. Conclusions

The present work aims to clarify and point out some links between several concepts in baroclinic instability, such as the underlying mathematical symmetries of the governing system, a mechanistic interpretation of the shear instability problem [e.g., 59–61, 66, 81], and geometric parameters of the eddy variance ellipses [e.g., 34, 36, 72]. We considered the Eady problem in the quasi-geostrophic system as a working example, modified to include a weak linear bottom slope. Making an assumption about the magnitude of slopes, the presence of the slope only affects the dynamics via a bottom boundary contribution to potential vorticity (PV), and the standard analysis leads to closed form solutions, as is known in the literature [e.g., 41–45, 53]. The resulting modified Eady system was claimed here to be parity-time ( $\mathcal{PT}$ ) symmetric [cf. 68–70, 81], with consequences for the the solution spectrum; we refer the reader to Appendix A for the full details and other more speculative links.

To clarify aspects of the edge-wave mechanism and the modification by the presence of a slope, we perform an edge-wave interaction analysis [cf., 61, 66, 71]. For the present system, where edge-wave locations are well-defined, the edge-wave analysis is really a rephrasing of the standard instability problem in a different choice of basis, and the standard modal instability problem is effectively one of finding fixed points of a two-dimensional dynamical system for the amplitude ratio and edge-wave phase-shift. Physically, we expect that for  $\delta < 0$ , where topographic slope and isentrope/isopycnals have horizontal gradients of opposite signs, more vertical stretching is allowed (cf. Fig. 1b), and thus it adds to the background PV gradient at the bottom. The bottom wave is then stronger, and its characteristic should be more apparent in the overall normal-modes. For  $\delta < 0$ ,  $c_r^\pm > 0 = c_r^\pm(\delta = 0)$  with our choice of basic state set up, since the bottom wave counter-propagates to the right (or east). The opposite is true for  $\delta > 0$ . The asymmetry is supported by the resulting edge-wave analysis, where the amplitude ratios are simply functions of  $\delta$  but not of the wavenumber (Fig. 5a); the dependence on  $\delta$  only should be expected from the PV point of view, but such a dependence is not in fact seen in the analysis of the tilted streamfunction eigenfunction (Fig. 6a).

The phase-shift of the edge-waves  $\Delta\epsilon$  associated with the most unstable mode is not necessarily at the theoretical optimum of  $\pi/2$  (actually slightly larger), and generically differs from the phase-tilt in the unstable streamfunction  $\Delta\epsilon_{\text{eigen}}$ , which does seem to be at  $\pi/2$  for  $\delta \leq 0$ . We argue that  $\Delta\epsilon$  rather than  $\Delta\epsilon_{\text{eigen}}$  should be the quantity of interest if a kinematic/mechanistic interpretation is to be invoked. The unstable normal-mode is a linear combination of the edge-wave structures (e.g. Fig. 4), and the phase-shifts in the untilted edge-waves structures do not have to correspond to the phase-tilts in the tilted streamfunction eigenfunctions. We are of the opinion that references to  $\Delta\epsilon_{\text{eigen}}$  should generally be avoided (an exception perhaps for the Phillips problem [13], where the entries of the normal-modes are defined as per-layer quantities and could be argued to already be in edge-wave form). If some reference is to be made to the energetics of the instability, the geometric parameters associated with eddy variance ellipses [e.g., 34, 60] such as buoyancy anisotropy  $\gamma_b$  serve as better measures of the correlation for the meridional velocity and buoyancy perturbations  $v'$  and  $b'$ . On the other hand, the vertical eddy tilt  $\phi_t$ , although defined with no reference to the edge-wave structures themselves, display characteristics of the edge-wave phase-shift  $\Delta\epsilon$ . The realized eddy efficiency parameter  $\alpha$  is shown to correlate strongly with the growth rate, in line with the definition given in [34]. It is found here that the dominant contribution to  $\alpha$  comes from  $\gamma_b$ , and so decreases in  $\alpha$  with variations in  $\delta$  arises the decrease in  $\gamma_b$ , consistent somewhat with previous diagnoses from a nonlinear realization of baroclinic dynamics in a numerical ocean model [82].

Previous works have argued that the changes in instability characteristics arises from changes in the edge-wave interaction, but only considers the need for phase-speed matching [53]. We argue that view is incomplete as the argument does not extend to all of parameter space, and does not explain all the instability characteristics. Here we clarify the mechanistic explanation. For  $\delta < 0$ , the bottom wave increases in strength, and not only does it intrinsically propagate faster (to the right or east), but leads to a larger action-at-a-distance. The top wave experiences a larger *hindering*, which can be compensated by reducing the vertical interaction function via moving to larger wavenumbers (which also reduces the intrinsic propagation speed of both edge-waves), and the weaker interaction function leads to weaker growth rates. It seems that it is always possible for such a compensation to be achieved in the  $\delta < 0$  case, albeit over a decreasing bandwidth. For  $\delta > 0$ , the opposite is true, except the reduction in interaction from the weakened bottom wave cannot be arbitrarily increased by moving to smaller wavenumbers, since that increases the intrinsic propagation speed of both edge waves. In this case the top edge-wave will become too fast for the given background flow and wave interaction for phase-locking to be possible. The instability bandwidth decreases in width and bounded away from the small wavenumber as  $\delta$  is increased towards 1. At  $\delta \geq 1$  there is no instability whatsoever, as counter-propagation of the bottom wave is no longer possible since the PV gradient vanishes or reverses sign.

Although the present work focuses largely on the zero meridional wavenumber case  $l = 0$ , the results and observations apply to the  $l \neq 0$  case. As a demonstration, the instability characteristics of  $l = 0.5$  with the meridional structure function  $g(y) = \sin(l y)$  is shown in Fig. 8. Here the instabilities generally possess weaker growth rates, with a change in the domain of instability in the  $\delta > 0$  region, but otherwise the general behavior of the growth rates and phase-speed  $c_r^\pm$  are similar to what has been reported (since the system is still  $\mathcal{PT}$  symmetric). The physical rationalization in terms of edge waves is still applicable. The reduction in growth rates can be attributed to weakened interaction from  $l \neq 0$ , since that increases the value of  $\mu = \text{Bu} \sqrt{k^2 + l^2}$ . The expanded domain of instability for  $\delta > 0$  can be rationalized as edge-waves having smaller intrinsic propagation speed in general (because of the increased  $\mu$ ), and so the top edge-wave can be held in a phase-locking configuration for the given basic flow, and the weakened interaction associated with weaker bottom edge-wave can in fact be compensated by increasing the interaction via decreasing the zonal wavenumber  $k$ . Edge-wave amplitude ratios  $\gamma$  is as given by (18), and the edge-wave phase-shift  $\Delta\epsilon$  has similar behavior to that observed in Fig. 5c (not shown). While the computation of the geometric parameters is slightly more complex as the relevant geometric variables are now two-dimensional, the conclusions and interpretations are essentially the same, except that the dominant contribution to  $\alpha$  now comes from  $\gamma_b \sin \phi_b$  (since  $R$  is no longer trivial and so  $\phi_b \neq \pm\pi/2$ ), but the energy partition contribution  $\sin 2\lambda$  is still close to 1 and largely constant over the domain. In particular, the vertical eddy tilt  $\phi_t$  follows the phase-shift of the edge-waves more so than the normal-mode phase-tilts (in terms of spatial distribution, average values down the center line, or domain-averaged values; not shown).

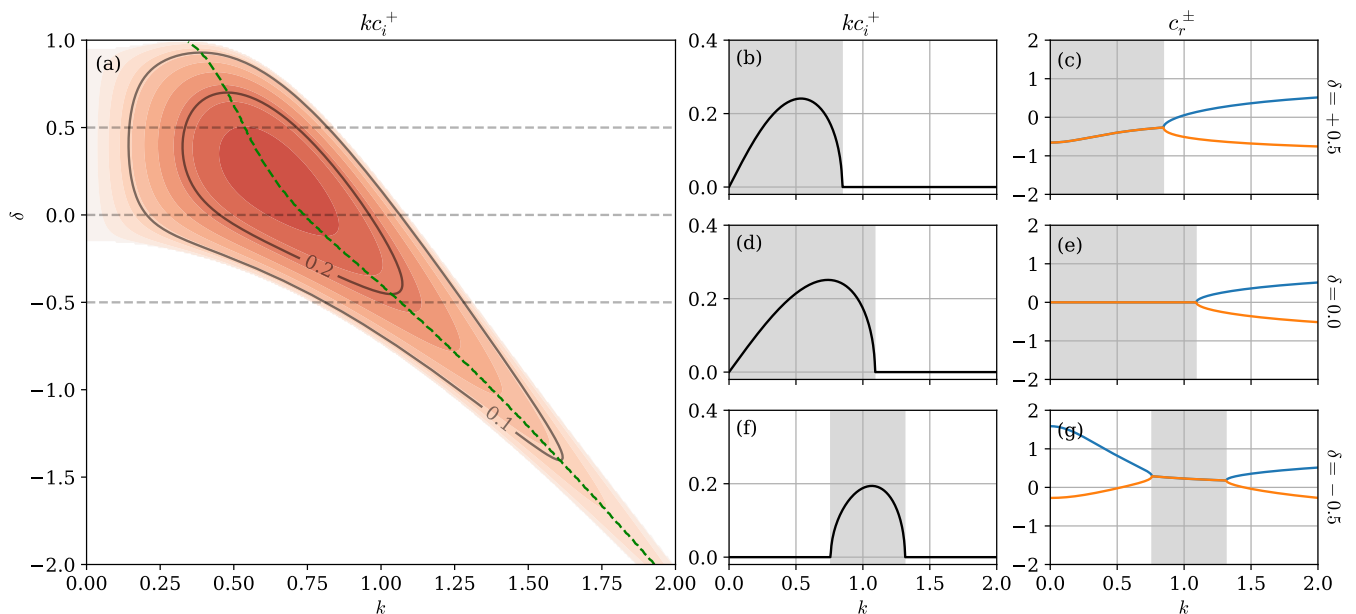


FIG. 8. Sample instability characteristics for  $l = 0.5$ , with the non-trivial meridional structure function  $g(y) = \sin(y/2)$ . (a) Growth rate as a function of the non-dimensional wavenumber  $k$  and  $\delta$  parameter, with darker shadings denoting higher values (strength of shading is the same used in Fig. 2), sample contours of growth rates, and the green dashed line denoting  $k_{\max}(\delta)$  where the growth rate is maximized. Also shown are the growth rates  $kc_i^\pm$  and phase-speed  $c_r^\pm$  for (b, c)  $\delta = +0.5$ , (d, e) the standard Eady problem  $\delta = 0.0$ , and (f, g)  $\delta = -0.5$ . The shaded regions in panels b-g denote the regions where there the growth rates are non-zero.

## B. Discussions and outlooks

The present work explores the behavior of the  $\alpha$  parameter from a linear instability point of view, to supplement parameterization efforts of particular relevance to ocean modeling. We find that there is indeed a suppression of  $\alpha$  in the presence of slopes, and the dominant contribution comes principally from changes in the buoyancy anisotropy parameter (as well as the eddy buoyancy angle where it is present). The result here would be consistent with previous observations that buoyancy fluxes are suppressed over sloped regions [e.g., 43, 44, 46, 48–53, 55], with previous diagnostic results but in the nonlinear regime in a realistic global ocean model [80], and is consistent with a parameterization that  $\alpha$  be suppressed over slopes in a way that is dependent on the slope Burger number [56], related to the  $\delta$  utilized in the present work. This work thus provides a consistency rationalization for the proposal of [56], which was empirical in nature. While the present work is for the linear regime, previous works have suggested that the linear instability characteristics can be useful in informing parameterizations that are invoked for the nonlinear regime [e.g., 29–33].

The stabilization of baroclinic instability in the presence of small slopes (related to the suppression of  $\alpha$ ) is rationalized in the PV point of view, where the presence of a slope modifies the background PV gradient and leads to modifications in the interaction of the Rossby edge-waves. The rationalization is given in Sec. III B, but is also summarized in the schematic given in Fig. 9. The point we clarify here is that it is the asymmetry in the wave amplitudes that lead to changes in the mutual interaction, that in turn modifies the phase-locking configuration, and the end result dictates a change in the phase-shift. Arguments based solely on phase-shifts and phase-speed matching is missing a key link in the interaction, and does not fully explain the instability characteristics over the whole parameter space. Further, we highlight that, from a mechanistic point of view, it is the untilted edge-wave basis and its phase-shift that is of relevance, and the phase-tilt in the tilted normal-modes is generally to be avoided as it can be misleading. The physical rationalization applies generically to baroclinic instability over slopes; sample analysis on the analogous Phillips problem [cf., 45] shows similar results and interpretations to here (not shown). It would further be interesting to see how some of the analysis and points of view (edge-waves and GEOMETRIC framework) here carry over to the case of transient / optimal growth [e.g., 83], but we leave this for a follow up study.

It was found that the vertical tilt angle  $\phi_t$  (rather than the buoyancy angle  $\phi_b$ ) possesses qualitative similarities to the edge-wave phase shifts, even though the former is defined with no reference to the edge-waves whatsoever. The observation is in line with the results in [72], who find that in the barotropic instability of the Rayleigh sheet that there is a relation between the horizontal tilt angles  $\phi_m$  (the momentum flux angles) and the edge-wave phase-shift. Then perhaps a parameterization of baroclinic instability could be based on the geometric parameters such as  $\phi_t$ , which informs the spatial structure of the eddy fluxes as well as an efficiency via  $\alpha$ , with a realized magnitude based on a parameterized eddy energy [cf. 34, 39]. For diagnostic



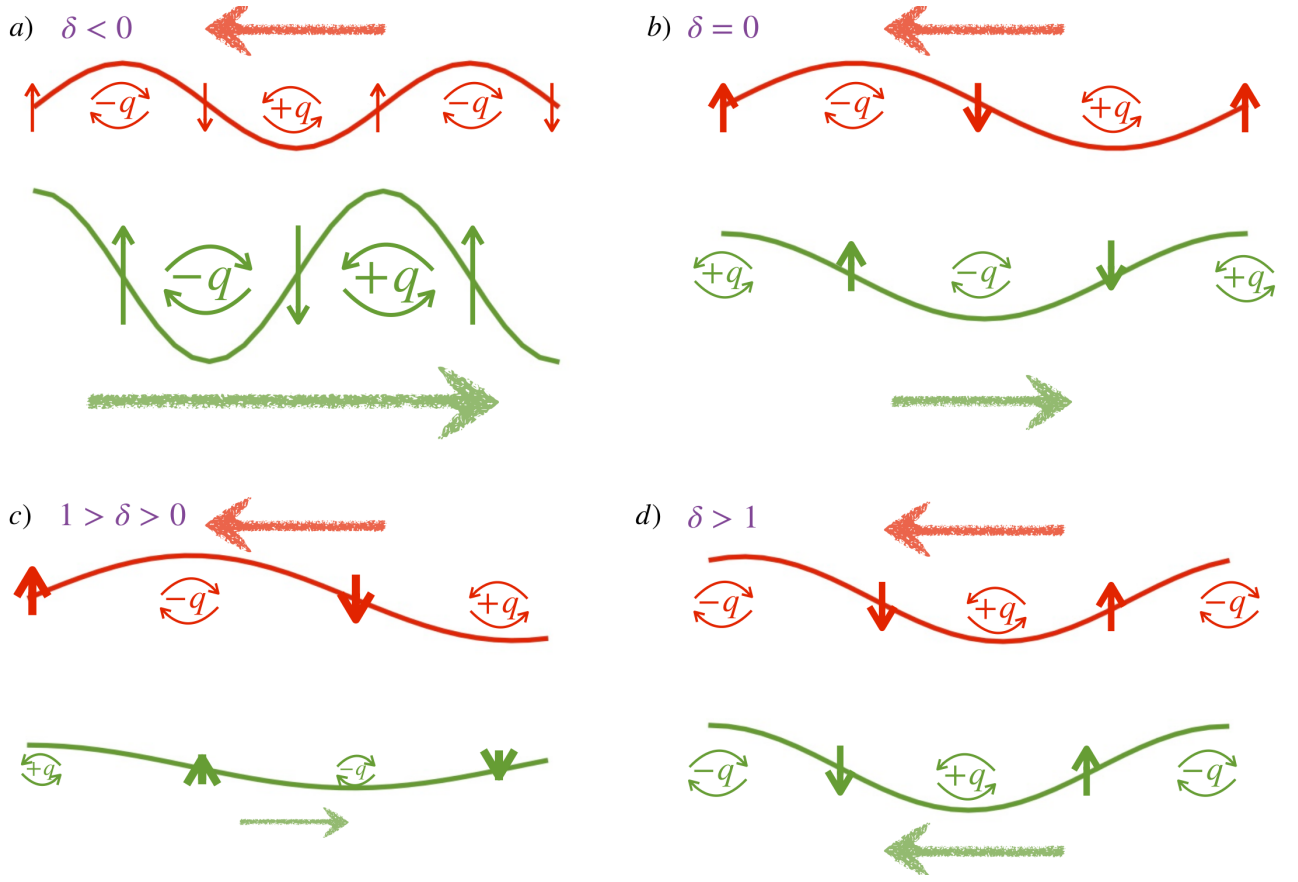


FIG. 9. Pictorial schematic for the change in instability characteristics over parameter space in terms of interacting Rossby edge-waves. (a) For the  $\delta < 0$  case, the bottom PV gradient is stronger, leading to a stronger bottom edge-wave that strengthens the magnitude of interaction and edge-wave propagation speed (represented by longer arrows), but this effect can be compensated by going to shorter waves (represented here by the thinner arrows). (b) The standard Eady case  $\delta = 0$ , where the interaction is symmetric. (c) For  $1 > \delta > 0$ , the bottom PV gradient weakens, leading to a weaker bottom edge-wave and a weaker interaction (represented by the shorter arrows), but this can be offset somewhat by going to longer waves (represented by the thicker arrows). (d) For  $\delta > 1$ , the PV gradient switches sign and the bottom edge-wave no longer counter-propagates against the background mean flow, no phase-locking configuration is possible, and there is no instability.

purposes, in cases where the edge-waves are not so well-defined (e.g., nonlinear cases, although see next paragraph), diagnoses of  $\phi_t$  could be done instead as a proxy for the phase-shift, since the geometric parameters considered here applies generically to cases where eddy fluxes can be diagnosed [34].

For the present linear problem the edge-waves are well-defined, and Sec. III provides a manual construction of the edge-wave basis (e.g., where one part of the edge-wave couplet has an untilted structure and no PV signal at the location of the other edge-wave). There are problems where edge wave structures are harder to define (e.g., instability in the presence of planetary  $\beta$  [11, 14, 72], the Rayleigh sheet problem in the presence of a magnetic field [65]), or cases where one might naturally expect linear theory to play no longer play a dominant role (e.g., during a nonlinear evolution). However, there are still ways to define an edge-wave basis, for example making use of orthogonality in the wave activity quantities such as pseudomomentum and pseudoenergy [e.g., 18, 61, 66, 73]. It is possible to extend the present analysis to some of the other models, such as the Charney–Green model, which has been pointed to possibly be more relevant than the Eady model in certain oceanic settings [e.g., 43, 46, 50, 52], problems with smooth profiles and/or profiles containing multiple PV gradients (e.g. jet profiles), and mixed barotropic-baroclinic problems [e.g., 84, 85]. In particular, if one believes that there is some sort of quasi-linear control on the linear instability on the nonlinear evolution, then perhaps the procedure will be illuminating for an analogous analysis for simulations of the nonlinear phase of the shear instabilities [e.g., 86]. These are left as possible future investigations to be pursued.

## ACKNOWLEDGMENTS

This work was supported by the the RGC General Research Fund 11308021 and the Center for Ocean Research in Hong Kong and Macau, a joint research center between the Laoshan Laboratory and Hong Kong University of Science and Technology. The Python Jupyter notebook used to generate and analyze data for the problem may be found at [https://github.com/julianmak/julianmak.github.io/blob/master/files/Eady/Eady\\_analysis.ipynb](https://github.com/julianmak/julianmak.github.io/blob/master/files/Eady/Eady_analysis.ipynb). GK was supported by a post-doctoral funding through the Center for Ocean Research in Hong Kong and Macau. Some of the work was initiated while EQYO was a visiting student at the Hong Kong University of Science and Technology. EQYO is supported by the Australian Government Research Training Program 678 Scholarship (RTP) and the Australian Research Council Special 676 Research Initiative, Australian Centre for Excellence in Antarctic Science (ARC project number 677 SR200100008). JM would like to thank Liyung Yeow and the hospitality of the staff at the Edison Hotel at Penang, Malaysia that lead to the discussion of  $\mathcal{PT}$ -symmetry in classical systems and the writing of the first draft of the present article.

Authorship is alphabetical after the first author. Resources, Supervision, Project administration, Funding acquisition: JM. Conceptualization, Visualization: JM, NH, EH. Methodology: JM, EH, GK. Software: JM, GK. Formal analysis: JM, NH, EH, GK. Writing - Original Draft: JM, NH, EH. Validation, Writing - Review & Editing: everyone.

### Appendix A: Parity-Time $\mathcal{PT}$ symmetry of the modified Eady problem

Note that in the text we made the observation that Eq. (3) is invariant under the transformation

$$\mathcal{P} : (x, y, z) \mapsto (-x, -y, -z), \quad \mathcal{T} : (t, \psi) \mapsto (-t, -\psi). \quad (\text{A1})$$

More formally, an operator  $\mathcal{H}$  governing a system is Parity-Time ( $\mathcal{PT}$ ) symmetric if it satisfies

$$(\mathcal{PT})\mathcal{H}^*(\mathcal{PT})^{-1} = \mathcal{H}, \quad (\text{A2})$$

where  $\mathcal{H}^*$  denotes the complex conjugate (rather than the Hermitian conjugate  $\mathcal{H}^\dagger$ , which for a matrix representation involves a transpose on top of the element-wise complex conjugate).

$\mathcal{PT}$  symmetry is a concept that originates from quantum physics [e.g., 67], but has found recent interest in classical fluid systems also [e.g., 68–70]. Here we show explicitly that the present modified Eady problem is  $\mathcal{PT}$  symmetric, which leads to certain features in the solution spectrum that was previously highlighted in Sec. II. The ideas and tools were previous given in the work of [70] for the Phillips-like problem (two layer QG with uniform flow in each layer, cf. [1, 13]). The following exposition is largely given for completeness, but also serves to highlight very suggestive links between  $\mathcal{PT}$  symmetry, shear instability and the edge-wave formalism, possibly enabling tools to be borrowed from quantum physics to further our understanding of classical fluid systems (e.g. nonlinear shear instability), or providing classical analogues with well-understood physics to complement the mathematical analysis of quantum systems.

Note that we can write the linearized system (3) in the form

$$\frac{\partial}{\partial t}\mathcal{L}\varphi = \mathcal{M}\varphi, \quad (\text{A3})$$

which is a generalized eigenvalue problem for the relevant operators  $\mathcal{L}$  and  $\mathcal{M}$  acting on an eigenfunction  $\varphi$ . If we are taking modal solutions as in (5), then  $\mathcal{L}$  has an explicit representation whose inverse that can in principle be computed for, and we can define  $M = \mathcal{L}^{-1}\mathcal{M}$  where

$$c\phi = M\phi, \quad (\text{A4})$$

with the eigenvector  $\phi = (a, b)$  in this case. For the system here, it can be shown that (using again the notation  $C = \cosh \mu$  and  $S = \sinh \mu$ )

$$L = \mu \begin{pmatrix} -S & C \\ S & C \end{pmatrix}, \quad L^{-1} = \frac{1}{2\mu CS} \begin{pmatrix} -C & C \\ S & S \end{pmatrix}, \quad M = \frac{-1}{SC} \begin{pmatrix} \frac{\delta}{2\mu}C^2 & \left(1 - \frac{\delta}{2}\right)\frac{CS}{\mu} - C^2 \\ \left(1 - \frac{\delta}{2}\right)\frac{CS}{\mu} - S^2 & \frac{\delta}{2\mu}S^2 \end{pmatrix}, \quad (\text{A5})$$

where  $L$  denotes the representation of  $\mathcal{L}$  when modal solutions (5) are taken.

In the present work,  $M$  is already real,  $\mathcal{PT}$  happens to be the negative identity in the matrix representation relevant for the present system [70], so  $M$  is  $\mathcal{PT}$ -symmetric. Another way to see that  $M$  is  $\mathcal{PT}$ -symmetric is to note that, for  $P$  and  $T$  denoting the matrix representations of  $\mathcal{P}$  and  $\mathcal{T}$ ,  $\mu$  is invariant under  $P : (k, l) \mapsto (-k, -l)$  (interpreting  $\mu = \text{Bu}|k|$  if  $l = 0$ ), while  $T$

introduces a minus sign through its action on the eigenvector  $\phi$ , but this is done twice, so since  $M$  is real, the above equality holds.

A particular consequence for  $M$  being  $\mathcal{PT}$  symmetric is that the entries  $M$  are all real (which we have manually demonstrated here in (A5), but is in fact a general feature). Further, the dispersion relation (A4), for a two component system, satisfies

$$c^2 - \text{Tr}(M) + \text{Det}(M) = 0, \quad c = \frac{1}{2} \left( \text{Tr}(M) \pm \sqrt{\text{Tr}(M)^2 - 4\text{Det}(M)} \right), \quad (\text{A6})$$

where the trace and determinant of  $M$  are given by

$$M = \begin{pmatrix} a_1 & a_2 \\ a_3 & a_4 \end{pmatrix}, \quad \text{Tr}(M) = a_1 + a_3, \quad \text{Det}(M) = a_1 a_4 - a_2 a_3.$$

The entries of  $M$  are given in (A5), and the resulting dispersion relation can be shown to coincide exactly with that given (7) obtained from standard means. Further, the eigenfunction of the system (defined up to some arbitrary constant) can be written as

$$\phi = \begin{pmatrix} a \\ b \end{pmatrix} = \begin{pmatrix} a_2 \\ -a_1 + \frac{1}{2} \left( \text{Tr}(M) \pm \sqrt{\text{Tr}(M)^2 - 4\text{Det}(M)} \right) \end{pmatrix}, \quad (\text{A7})$$

and the eigenfunction  $\phi$  is  $\mathcal{PT}$ -symmetric if  $\phi$  is real. However, for the eigenvector of an unstable mode in the present system,  $\text{Tr}(M)^2 - 4\text{Det}(M) < 0$ , and the resulting eigenvector becomes complex and ceases being an eigenfunction of the  $\mathcal{PT}$  operator (because there is an extra minus introduced under a complex conjugate of the eigenvector), and we have what is termed *spontaneous breaking of  $\mathcal{PT}$ -symmetry*. The boundary between the region with and without spontaneous  $\mathcal{PT}$ -symmetry breaking are called *exceptional points*, and these correspond precisely to the locations of marginal stability. The collision of eigenvalues  $c^\pm$  on the real axis into complex conjugates is related to what are known as *Krein collisions* [e.g., 67, 69].

It is perhaps easy to see that, using the same framework of [70], other shear flow instability problems should also be  $\mathcal{PT}$  symmetric, such as Phillips-like problems [cf., 45, 70], Charney–Green-like problems [cf. 1, 11, 14], the standard Rayleigh sheet problem [81] in hydrodynamics, the Rayleigh sheet problem in magnetohydrodynamics with a uniform background magnetic field [e.g., 65], and more general shear flow problems presumably. Additionally, given the link between shear instabilities and its physical interpretation as a pair of interacting edge-waves, one is left to wonder on the exact links between  $\mathcal{PT}$  symmetry and interacting edge waves. Suggestive links include that spontaneous breaking of  $\mathcal{PT}$  symmetry seems to correspond exactly to when phase-locking occurs [cf., 70]. A Krein collision of the eigenvalue occurs at exception points requires opposite signed Krein signatures, reminiscent of the requirement that shear instabilities require modes of opposite signed wave activity to collide (as positive/negative energy modes [87] or pseudomomentum [e.g., 73]), which is sometimes interpreted as a necessary (but not sufficient) condition for instability is the need for counter-propagation of edge-waves [e.g., 61].

While an explicit link to the edge-wave system with  $\mathcal{PT}$  symmetry has been highlighted in the recent work of [81], and low-dimensional edge-wave systems (low-dimensional in the sense of dynamical systems) could be considered as a rephrasing of certain shear instability problem [e.g., 61], the links with the general shear instability problem for general shear flows remain to be explored (since generic shear flow instability problems should be regarded an infinite dimensional dynamical system). For example, what is the analogue of the Krein signature of the modes of the governing operator in the more standard fluid dynamics context? (Likely something related to pseudomomentum or pseudoenergy?) How are the standard shear flow linear stability conditions related to the properties of the governing operator, and in terms of interacting edge-waves? (Related to proofs of a purely real spectrum in  $\mathcal{PT}$  symmetric systems [e.g., 88, 89]?) Are there conditions beyond the standard necessary but not sufficient conditions of shear instability derivable from the  $\mathcal{PT}$  symmetry property, using techniques drawn from quantum physics? Most references of  $\mathcal{PT}$  symmetry in relation to shear instability systems so far is on the linear problem, but are there nonlinear analogues of the stability conditions such as the Arnol'd conditions [e.g., 18] derivable from a similar approach? Such links could in principle provide a mechanistic/physical interpretation to a theoretical properties related to  $\mathcal{PT}$  symmetry, and techniques in relation to analyzing  $\mathcal{PT}$  symmetric systems from quantum physics could provide new approaches for improving our understanding of classical fluid/plasma systems. The role of  $\mathcal{PT}$  symmetry for fluid/plasma systems remains to be fully explored, and research in this direction is a subject of future work.

---

[1] G. K. Vallis, *Atmospheric and Oceanic Fluid Dynamics* (Cambridge University Press, 2006).

[2] R. V. E. Lovelace, H. Li, S. A. Colgate, and A. F. Nelson, Rossby wave instability of Keplerian accretion disks, *Astrophys. J.* **513**, 805 (1999).

[3] Y. Kaspi and G. R. Flierl, Formation of jets by baroclinic instability on gas planet atmospheres, *J. Atmos. Sci.* **64**, 3177 (2007).

[4] D. W. Hughes, R. Rosner, and N. O. Weiss, *The solar tachocline* (Cambridge University Press, 2007).

- [5] R. J. Teed, C. A. Jones, and R. Hollerbach, Rapidly rotating plane layer convection with zonal flow, *Geophys. Astrophys. Fluid Dyn.* **104**, 457 (2010).
- [6] I. Polichtchouk and J. Y. Cho, Baroclinic instability on hot extrasolar planets, *Mon. Not. R. Astron. Soc.* **424**, 1307 (2012).
- [7] P. A. Gilman and M. Dikpati, Baroclinic instability in the solar tachocline, *Astrophys. J.* **787**, 60 (1402).
- [8] P. A. Gilman, Effect of toroidal fields on baroclinic instability in the solar tachocline, *Astrophys. J.* **801**, 22 (2015).
- [9] P. Read, D. Kennedy, N. Lewis, H. Scolan, F. Tabataba-Vakili, Y. Wang, S. Wright, and R. Young, Baroclinic and barotropic instabilities in planetary atmospheres: energetics, equilibration and adjustment, *Nonlin. Processes Geophys.* **27**, 147 (2020).
- [10] R. Yellin-Bergovoy, O. M. Umurhan, and E. Heifetz, A minimal model for vertical shear instability in protoplanetary accretion disks, *Geophys. Astrophys. Fluid Dyn.* **115**, 674 (2021).
- [11] J. G. Charney, Dynamics of long waves in a baroclinic westerly current, *J. Meteor.* **4**, 135 (1947).
- [12] E. T. Eady, Long waves and cyclone waves, *Tellus* **1**, 33 (1949).
- [13] N. A. Phillips, The general circulation of the atmosphere: a numerical experiment, *Q. J. Roy. Met. Soc.* **82**, 123 (1956).
- [14] J. S. A. Green, A problem in baroclinic instability, *Q. J. Roy. Met. Soc.* **86**, 237 (1960).
- [15] J. G. Charney and M. E. Stern, On the stability of internal baroclinic jets in a rotating atmosphere, *J. Atmos. Sci.* **19**, 159 (1962).
- [16] J. Pedlosky, The stability of currents in the atmosphere and the ocean: Part I, *J. Atmos. Sci.* **21**, 201 (1964).
- [17] J. Pedlosky, The stability of currents in the atmosphere and the ocean: Part II, *J. Atmos. Sci.* **21**, 342 (1964).
- [18] T. G. Shepherd, Symmetries, conservation laws, and Hamiltonian structure in geophysical fluid dynamics, *Adv. Geophys.* , 287 (1990).
- [19] T. G. Shepherd, Nonlinear saturation of baroclinic instability: part I: the two-layer model, *J. Atmos. Sci.* **45**, 2014 (1990).
- [20] T. G. Shepherd, Nonlinear saturation of baroclinic instability: part II: continuous stratified fluid, *J. Atmos. Sci.* **46**, 888 (1990).
- [21] C. D. Thorncroft, B. J. Hoskins, and M. E. McIntyre, Two paradigms of baroclinic-wave life-cycle behaviour, *Q. J. Roy. Met. Soc.* **119**, 17 (1993).
- [22] V. D. Larichev and I. M. Held, Eddy amplitudes and fluxes in a homogeneous model of fully developed baroclinic instability, *J. Phys. Oceanogr.* **25**, 2285 (1995).
- [23] M. A. Spall and D. C. Chapman, On the efficiency of baroclinic eddy heat transport across narrow fronts, *J. Phys. Oceanogr.* **28**, 2275 (1998).
- [24] A. F. Thompson and W. R. Young, Two-layer baroclinic eddy heat fluxes: Zonal flows and energy balance, *J. Atmos. Sci.* **64**, 3214 (2007).
- [25] J. G. Esler, The turbulent equilibration of an unstable baroclinic jet, *J. Fluid Mech.* **599**, 241 (2008).
- [26] S. D. Bachman and B. Fox-Kemper, Eddy parametrization challenge suite I: Eady spindown, *Ocean Modell.* **64**, 12 (2013).
- [27] S. D. Bachman, D. P. Marshall, J. R. Maddison, and J. Mak, Evaluation of a scalar transport coefficient based on geometric constraints, *Ocean Modell.* **109**, 44 (2017).
- [28] C. Chang and I. M. Held, A scaling theory for the diffusivity of poleward eddy heat transport based on Rhines scaling and the global entropy budget, *J. Atmos. Sci.* **79**, 1743 (2022).
- [29] J. S. A. Green, Transfer properties of the large-scale eddies and the general circulation of the atmosphere, *Q. J. Roy. Met. Soc.* **96**, 157 (1970).
- [30] P. H. Stone, A simplified radiative-dynamical model for the static stability of rotating atmospheres, *J. Atmos. Sci.* **29**, 405 (1972).
- [31] P. D. Killworth, On the parameterization of eddy transfer, Part I. Theory, *J. Mar. Res.* **55**, 1171 (1997).
- [32] P. D. Killworth, On the parameterization of eddy transfer, Part II. Tests with a channel model, *J. Mar. Res.* **56**, 349 (1998).
- [33] C. Eden, A closure for meso-scale eddy fluxes based on linear instability theory, *Ocean Modell.* **39**, 362 (2011).
- [34] D. P. Marshall, J. R. Maddison, and P. S. Berloff, A framework for parameterizing eddy potential vorticity fluxes, *J. Phys. Oceanogr.* **42**, 539 (2012).
- [35] J. R. Maddison and D. P. Marshall, The Eliassen–Palm flux tensor, *J. Fluid Mech.* **729**, 69 (2013).
- [36] B. J. Hoskins, I. N. James, and G. H. White, The shape, propagation and mean-flow interaction of large-scale weather systems, *J. Atmos. Sci.* **40**, 1595 (1985).
- [37] S. Waterman and B. J. Hoskins, Eddy shape, orientation, propagation, and mean flow feedback in western boundary current jets, *J. Phys. Oceanogr.* **43**, 1666 (2013).
- [38] J. Mak, J. R. Maddison, D. P. Marshall, and D. R. Munday, Implementation of a geometrically informed and energetically constrained mesoscale eddy parameterization in an ocean circulation model, *J. Phys. Oceanogr.* **48**, 2363 (2018).
- [39] J. Mak, D. P. Marshall, G. Madec, and J. R. Maddison, Acute sensitivity of global ocean circulation and heat content to eddy energy dissipation time-scale, *Geophys. Res. Lett.* **49**, e2021GL097259 (2022).
- [40] J. Mak, J. R. Maddison, D. P. Marshall, X. Ruan, and Y. Wang, Scale-awareness in an eddy energy constrained mesoscale eddy parameterization, *J. Adv. Model. Earth. Syst.* **15**, e2023MS003886 (2023).
- [41] S. K. Blumsack and P. Gierasch, Mars: The effects of topography on baroclinic instability, *J. Atmos. Sci.* **29**, 1081 (1972).
- [42] C. R. Mechoso, Baroclinic instability of flows along sloping boundaries, *J. Atmos. Sci.* **37**, 1393 (1980).
- [43] P. E. Isachsen, Baroclinic instability and eddy tracer transport across sloping bottom topography: How well does a modified Eady model do in primitive equation simulations?, *Ocean Modell.* **39**, 183 (2011).
- [44] K. Brink, Baroclinic instability of an idealized tidal mixing front, *J. Mar. Res.* **70**, 661 (2012).
- [45] C. Chen and I. Kamenkovich, Effects of topography on baroclinic instability, *J. Phys. Oceanogr.* **43**, 790 (2013).
- [46] P. E. Isachsen, Baroclinic instability and the mesoscale eddy field around the Lofoten Basin, *J. Geophys. Res. Oceans* **120**, 2884 (2015).
- [47] J. Pedlosky, Baroclinic instability over topography: Unstable at any wave number, *J. Mar. Res.* **74**, 1 (2016).
- [48] G. E. Manucharyan, A. F. Thompson, and M. A. Spall, Eddy-Memory mode of multi-decadal variability in residual-mean ocean circulations with application to the Beaufort Gyre, *J. Phys. Oceanogr.* **47**, 855 (2017).
- [49] R. D. Hetland, Suppression of baroclinic instabilities in buoyancy-driven flow over sloping bathymetry, *J. Phys. Oceanogr.* **47**, 49 (2017).
- [50] M. Trodahl and P. E. Isachsen, Topographic influence on baroclinic instability and the mesoscale eddy field in the northern North Atlantic Ocean and the Nordic seas, *J. Phys. Oceanogr.* **48**, 2593 (2018).

- [51] Y. Wang and A. L. Stewart, Eddy dynamics over continental slopes under retrograde winds: Insights from a model inter-comparison, *Ocean Modell.* **121**, 1 (2018).
- [52] G. E. Manucharyan and P. E. Isachsen, Critical role of continental slopes in halocline and eddy dynamics of the Ekman-driven Beaufort Gyre, *J. Geophys. Res. Oceans* **124**, 2679 (2019).
- [53] S. Chen, C. Chen, and J. A. Lerczak, On baroclinic instability over continental shelves: Testing the utility of Eady-type models, *J. Phys. Oceanogr.* **50**, 3 (2020).
- [54] Y. Tanaka, Stability of a flow over bottom topography: A general condition and a linear analysis in a two-layer quasi-geostrophic model with a possible application to a Kuroshio meander, *J. Geophys. Res. Oceans*. **126**, e2021JC017849 (2021).
- [55] H. Wei and Y. Wang, Full-depth scalings for isopycnal eddy mixing across continental slopes under upwelling-favorable winds, *J. Adv. Model. Earth. Syst.* **13**, e2021MS002498 (2021).
- [56] H. Wei, Y. Wang, A. L. Stewart, and J. Mak, Scalings for eddy buoyancy fluxes across prograde shelf/slope fronts, *J. Adv. Model. Earth. Syst.* **14**, e2022MS003229 (2022).
- [57] H. Wei, Y. Wang, and J. Mak, Parameterizing eddy buoyancy fluxes across prograde shelf/slope fronts using a slope-aware GEOMETRIC closure, *J. Phys. Oceanogr.* **54**, 359 (2024).
- [58] A. Nummelin and P. E. Isachsen, Parameterizing mesoscale eddy buoyancy transport over sloping topography, *ESS Open Archive* 10.22541/essoar.168394750.04852652/v2 (2024).
- [59] F. P. Bretherton, Baroclinic instability and the short wavelength cut-off in terms of potential vorticity, *Q. J. Roy. Met. Soc.* **92**, 335 (1966).
- [60] B. J. Hoskins, M. E. McIntyre, and A. W. Robertson, On the use and significance of isentropic potential vorticity maps, *Q. J. Roy. Met. Soc.* **111**, 877 (1985).
- [61] E. Heifetz, C. H. Bishop, B. J. Hoskins, and J. Methven, The counter-propagating Rossby-wave perspective on baroclinic instability. I: Mathematical basis, *Q. J. Roy. Met. Soc.* **130**, 211 (2004).
- [62] E. Heifetz, C. H. Bishop, and P. Alpert, Counter-propagating Rossby waves in the barotropic Rayleigh model of shear instability, *Q. J. Roy. Met. Soc.* **125**, 2835 (1999).
- [63] N. Harnik and E. Heifetz, Relating overreflection and wave geometry to the counter-propagating Rossby wave perspective: Toward a deeper mechanistic understanding of shear instability, *J. Atmos. Sci.* **64**, 2238 (2007).
- [64] A. Rabinovich, O. M. Umurhan, N. Harnik, F. Lott, and E. Heifetz, Vorticity inversion and action-at-a-distance instability in stably stratified shear flow, *J. Fluid Mech.* **670**, 301 (2011).
- [65] E. Heifetz, J. Mak, J. Nycander, and O. M. Umurhan, Interacting vorticity waves as an instability mechanism for magnetohydrodynamic shear instabilities, *J. Fluid Mech.* **767**, 199 (2015).
- [66] E. Heifetz and A. Guha, Normal form of synchronization and resonance between vorticity waves in shear flow instability, *Phys. Rev. E* **100**, 043105 (2019).
- [67] C. M. Bender, *PT Symmetry: In Quantum And Classical Physics*, 1st ed. (World Scientific, 2018).
- [68] H. Qin, R. Zhang, A. S. Glasser, and J. Xiao, Kelvin-Helmholtz instability is the result of parity-time symmetry breaking, *Phys. Plasma* **26**, 032102 (2019).
- [69] R. Zhang, H. Qin, and J. Xiao, PT-symmetry entails pseudo-Hermiticity regardless of diagonalizability, *J. Math. Phys.* **61**, 012101 (2020).
- [70] T. W. David, P. Delplace, and A. Venaille, How do discrete symmetries shape the stability of geophysical flows?, *Phys. Fluids* **34**, 056605 (2022).
- [71] H. C. Davies and C. H. Bishop, Eady edge waves and rapid development, *J. Atmos. Sci.* **51**, 1930 (1994).
- [72] T. Tamarin, J. R. Maddison, E. Heifetz, and D. P. Marshall, A geometric interpretation of eddy Reynolds stresses in barotropic ocean jets, *J. Phys. Oceanogr.* **46**, 2285 (2016).
- [73] I. M. Held, Pseudomomentum and the orthogonality of modes in shear flows, *J. Atmos. Sci.* **42**, 2280 (1985).
- [74] E. Heifetz, N. Harnik, and T. Tamarin, Canonical hamiltonian representation of pseudoenergy in shear flows using counter-propagating rossby waves, *Q. J. Roy. Met. Soc.* **135**, 2161 (2009).
- [75] S. H. Strogatz, *Nonlinear Dynamics And Chaos: With Applications To Physics, Biology, Chemistry, And Engineering (Studies in Nonlinearity)*, 1st ed. (CRC Press, 2000).
- [76] E. Heifetz and A. Guha, A generalized action-angle representation of wave interaction in stratified shear flows, *J. Fluid Mech.* **834**, 220 (2017).
- [77] N. Nakamura, Momentum flux, flow symmetry, and the nonlinear barotropic governor, *J. Atmos. Sci.* **50**, 2159 (1993).
- [78] S. Waterman and J. M. Lilly, Geometric decomposition of eddy feedbacks in barotropic systems, *J. Phys. Oceanogr.* **45**, 1009 (2015).
- [79] M. K. Youngs, A. F. Thompson, A. Lazar, and K. J. Richards, ACC meanders, energy transfer, and mixed barotropic-baroclinic instability, *J. Phys. Oceanogr.* **47**, 1291 (2017).
- [80] M. B. Poulsen, M. Jochum, J. R. Maddison, D. P. Marshall, and R. Nuterman, A geometric interpretation of Southern Ocean eddy form stress, *J. Phys. Oceanogr.* **49**, 2553 (2019).
- [81] C. Meng and Z. Guo, Vorticity wave interaction and exceptional points in shear flow instabilities (2023), arXiv:2303.11842 [physics.flu-dyn].
- [82] K. D. Stewart, P. Spence, S. Waterman, J. Le Sommer, J.-M. Molines, J. M. Lilly, and M. H. England, Anisotropy of eddy variability in the global ocean, *Ocean Modell.* **95**, 53 (2015).
- [83] E. Heifetz and J. Methven, Relating optimal growth to counter-propagating Rossby Waves in shear instability, *Phys. Fluids* **17**, 064107 (2005).
- [84] I. N. James, Suppression of baroclinic instability in horizontally sheared flows, *J. Atmos. Sci.* **44**, 3710 (1987).
- [85] N. Nakamura, An illustrative model of instabilities in meridionally and vertically sheared flows, *J. Atmos. Sci.* **50**, 357 (1993).
- [86] N. Harnik, D. G. Dritschel, and E. Heifetz, On the equilibration of asymmetric barotropic instability, *Q. J. Roy. Met. Soc.* **140**, 2444 (2014).
- [87] R. A. Cairns, The role of negative energy waves in some instabilities of parallel flows, *J. Fluid Mech.* **92**, 1 (1979).

- [88] P. Dorey, C. Dunning, and R. Tateo, Spectral equivalences, Bethe ansatz equations, and reality properties in PT-symmetric quantum mechanics, *J. Phys. A Math.* **34**, 5679 (2001).
- [89] A. Mostafazadeh, Pseudo-Hermiticity versus PT symmetry: The necessary condition for the reality of the spectrum of a non-Hermitian Hamiltonian, *J. Math. Phys.* **43**, 205 (2002).